8-9-2014

GARZÓN MASSIF BASEMENT TECTONICS: A GEOPYHYSICAL STUDY, UPPER MAGDALENA VALLEY, COLOMBIA

Kadir Baris Bakioglu
University of South Carolina - Columbia

GARZÓN MASSIF BASEMENT TECTONICS: A GEOPYHYSICAL STUDY, UPPER MAGDALENA VALLEY, COLOMBIA

by

Kadir Baris Bakioglu

Bachelor of Science
Sakarya University, 2009

Submitted in Partial Fulfillment of the Requirements

For the Degree of Master of Science in

Geological Sciences

College of Arts and Sciences

University of South Carolina

2014

Accepted by:

James N. Kellogg, Director of Thesis

Scott White, Reader

Pradeep Talwani, Reader

Lacy Ford, Vice Provost and Dean of Graduate Studies

DEDICATION

This work is in honor of my parents, Ali & Bilsen Bakioglu, my beloved wife Krystal, who always supported me with great patience, and in loving memory of Kemal Ataturk, the founder of the Modern Turkish Republic for a better future with peace and prosperity.

ACKNOWLEDGEMENTS

This research was initiated with partial funding from Emerald Energy Colombia Public Limited Company, Bogota, Colombia. The study took place in the Andean Geophysical Lab in the Department of Earth and Ocean Sciences at the University of South Carolina. The aerial gravity and aeromagnetic data were provided by Agencia Nacional de Hidrocarburos, the Colombian National Hydrocarbon Agency. Seismic reflection and well data for the project were provided by Emerald Energy Colombia. I especially would like to thank Edgar Guerrero Enriquez from Emerald Energy for his support and help.

The theory and method of investigation of the research evolved based on the thoughtful comments and recommendations of the members of my thesis committee, Dr. Scott White and Dr. Pradeep Talwani.

I owe a special thanks to my faculty advisor Dr. James N. Kellogg who suggested this fascinating project and for his scientific and moral support. Additionally, it would be unfair not to mention the staff of the Andean Geophysical Laboratory who provided me with technical support as well as their scientific perspectives in a friendly atmosphere.

Last, but not least, I would not have had this opportunity without the full Graduate Fellowship from the Turkish National Education Ministry and Turkish Petroleum Corporation, which will be part of my life after graduation.

ABSTRACT

The mechanics and kinematics of basement tectonic uplifts, such as the Laramide Rocky Mountain orogeny, remain poorly understood and controversial. The debate continues in part because of the limited number of well-documented present day analogs. The Garzón Massif rising between the Upper Magdalena Valley and the Llanos Basin of Colombia is an active basement uplift with well, seismic, gravity, and magnetic data available. In the past 10 Ma, PreCambrian age granitic rocks of the Garzón Massif have been uplifted and displaced against Cretaceous and Tertiary sediments of the Upper Magdalena Valley along the Garzón fault.

Aerogravimetric data calibrated by well data and 2D seismic data were used to model the geometry of the Garzón fault and the top of basement (Saldaña Fm) in 2 dimensions. The density models provide an independent estimate of fault orientation. A high density airborne gravity and magnetic survey were flown over the Garzón fault in 2000, including 2,663 line km along 1 x 5 and 1 x 4 km flight lines at elevations of 2564 and 4589 m above mean sea level.

An initial depth model was derived from the well logs, seismic reflection profile, and down-hole velocity surveys. Airborne gravity data was used to produce a Bouguer anomaly gravity map. Average rock densities were estimated from density logs, seismic velocities, and formation rock types. The regional gravity field was estimated and two-

Dimensional forward models were constructed with average densities from the wells, seismic velocities, and rock types, and the initial depth model. Since the model fit is dependent on the density assumed for the Garzón Massif rocks, multiple densities and dip angles were tested.

The gravity analysis indicates that the Garzón fault is a basement thrust fault dipping at a shallow angle under the Massif. Best-fit models show a true dip of 12 to 17 degrees to the southeast. A regional density and magnetic susceptibility model of the entire Massif is consistent with dense basement rocks throughout the Garzón Massif and asymmetric loading (sedimentary basin is much deeper on NW flank – Upper Magdalena Valley). Crust thickens to the NW toward the Central Cordillera. Euler deconvolution of the magnetic field shows pronounced NE-SW trending features under the Massif which are interpreted as faults bounding a possible pre-Cambrian sedimentary rift graben. Retrodeformed 2D regional models indicate 13 km of shortening on the Garzón basement thrust in the last 12 Ma. Approximately 9 km of shortening occurred on the SE marginal basement thrust fault, probably also in the last 12 Ma. This was preceded by approximately 43 km of shortening by thin-skinned imbricate thrusting to the southeast (12 - 25 Ma). This study provides a well-documented example of an active basement uplift on low angle thrust faults.

TABLE OF CONTENTS

LIST OF TABLES

LIST OF FIGURES

CHAPTER 1: INTRODUCTION

The mechanics and kinematics of basement tectonic uplifts, such as the Laramide Rocky Mountain orogeny, remain poorly understood and controversial. The debate continues in part because of the paucity of well-documented present day analogs. The Garzón Massif rising between the Upper Magdalena Valley and the Llanos Basin of Colombia is an active basement uplift with well, seismic, gravity, and magnetic data available. In the past 10 Ma, PreCambrian age granitic rocks of the Garzón Massif have been uplifted and displaced against Cretaceous and Tertiary sediments of the Upper Magdalena Valley along the Garzón fault.

Aerogravimetric data calibrated by well data and 2D seismic data was used to model the geometry of the Garzón fault and the top of basement (Saldaña Fm) in 2 dimensions. The density models provide an independent estimate of fault orientation. A high density airborne gravity and magnetic survey was flown over the Garzón fault in 2000, including 2,663 line km along 1 x 5 and 1 x 4 km flight lines at elevations of 2564 and 4589 m above mean sea level.

An initial depth model was derived from the well logs, seismic reflection profile, and down-hole velocity surveys. Airborne gravity data was used to produce a Bouguer anomaly gravity map. Average rock densities were estimated from density logs,

seismic velocities, and formation rock types. The regional gravity field was estimated and 2-dimensional forward models were constructed with average densities from the wells, seismic velocities, and rock types, and the initial depth model. Since the model fit is dependent on the density assumed for the Garzón Massif rocks, multiple densities and dip angles were tested, and the errors between calculated and observed were compared for 11 densities and 8 dip angles (88 models).

Our gravity analysis indicates that the Garzón fault is a basement thrust fault dipping at a shallow angle under the Massif. This study provides a well-documented example of an active basement uplift by low angle thrust faulting. A regional profile tests whether the uplift is symmetric or asymmetric, and constrains the extent of basement involvement, the depth of the Garzón fault, and orogenic uplift and shortening.

1.1 Kinematics and mechanics of basement thrust faults

Empirical observations of the mechanical failure of rocks in the shallow crust can be explained by the magnitude of the differential stresses acting on a rock volume as shown in the Mohr diagram (Figure 1.1). Subsequently, The Mohr diagrams were modified to account for the cohesiveness of rocks with the Mohr – Coulomb failure criterion ($\tau = C + \sigma\mu$ where τ is the shear stress, C is the cohesive shear stress, σ is the normal stress and μ is the angle of the rock friction, Figures 1.2 and 1.3). The Mohr – Coulomb failure envelope can be applied to geological engineering problems related to soil mechanics as well as geological problems such as fault geometries for three failure modes: tensional fracturing, tensional – transitional fracturing and compressional shear failure (Figure 1.2).

Anderson (1905) used the Coulomb – Mohr theory to explain the geometry of faults in specific shear failure and fracturing systems. Close to the Earth's surface, one of the principal stresses will be vertical, whereas the remaining two principal stresses are horizontal.

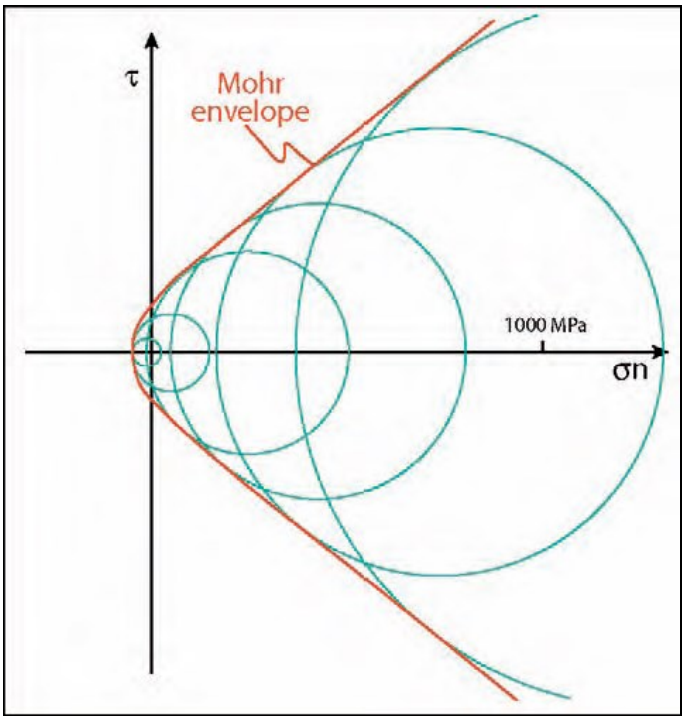

Figure 1.1: Mohr diagram showing the state of effective stress at failure for various experiments. Each circle represents the state of stress at failure at a different mean stress. The locus of stress states that bounds the field of stable and unstable stresses is called the Mohr envelope.

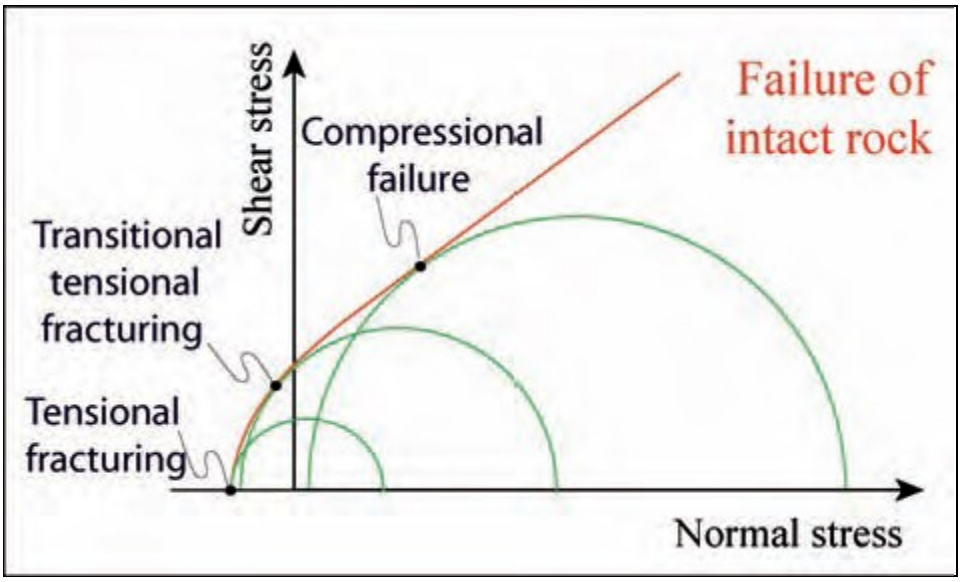

Figure 1.2: Generic Mohr diagram showing a composite Griffith – Coulomb failure envelope for intact rocks. The three shown critical stress circles represent different failure modes.

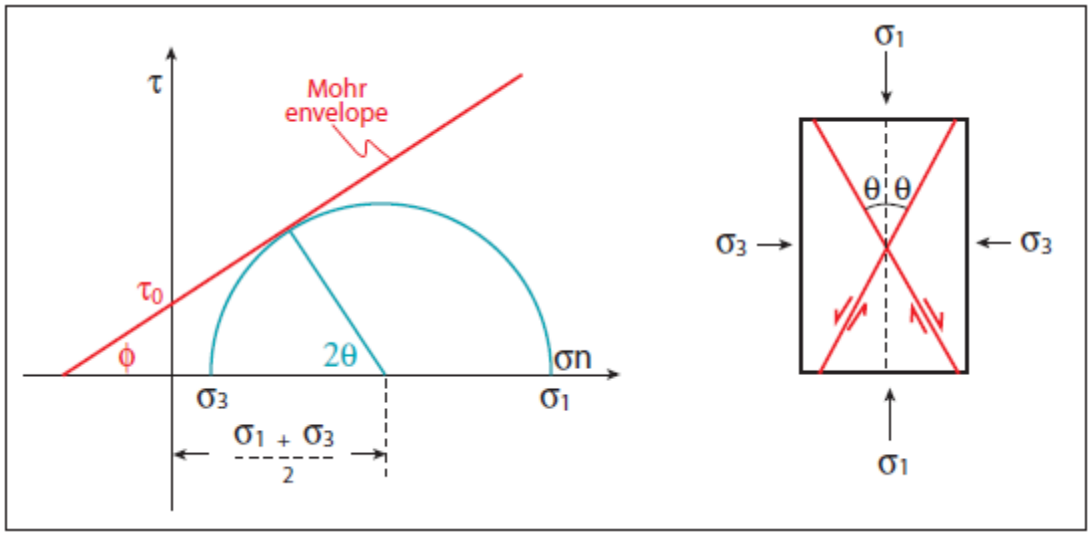

Figure 1.3: Mohr – Coulomb failure criterion for isotopic intact rocks (left panel). The point of tangency of the Mohr circle represents the state of stress on the plane which is at angle θ from the σ_1 axis of the right panel.

According to Anderson`s theory, the main compressional stress σ_1 is vertical in extensional regimes and normal faults usually develop with high dip angles (approximately 60°), whereas it is horizontal in contractional areas and thrust faults

develop with low angle dips (around 30º). Strike-slip settings are controlled with σ_2 vertical principal stress and strike – slip faults are mainly subvertical (Figure 1.4).

Hubbert (1961) showed that Anderson's theory was also applicable to empirical results of faulting in loose sand. Hubbert's (1961) results for reverse faults in sand produced remarkably consistent dip angles (25.1° ± 2.6º, Table 1.1).

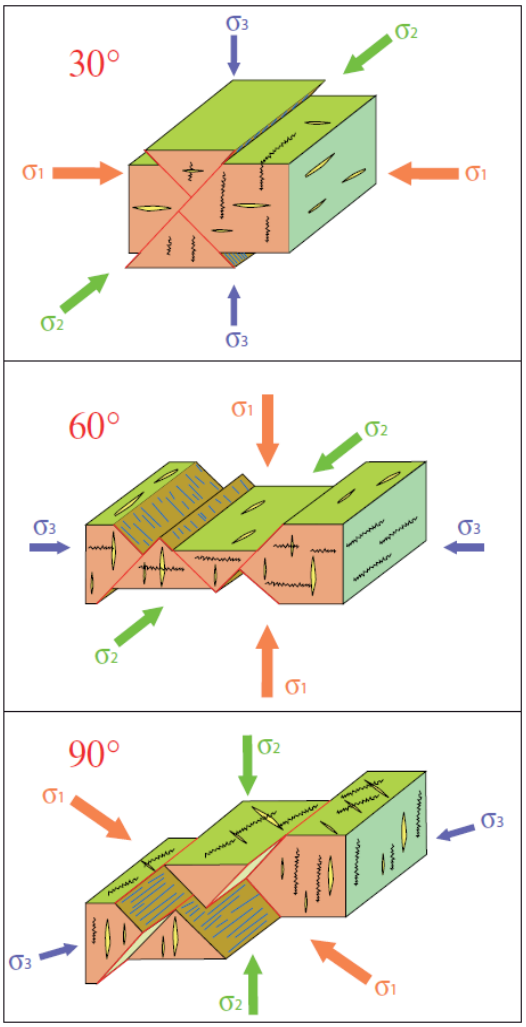

Figure 1.4: Anderson`s theory of faulting for contractional (top), extensional (middle) and shear faulting (bottom) (Modified from Hubbert ,1961).

Table 1.1: Results of Hubbert (1961) dip angles for reverse faults in sand experiment.

Experiment No.	Angle of Dip
1	23
2	22
3	28
4	23
5	25
6	28
7	27
8	26.5
9	26.5
10	29.5
11	24.5
12	22
13	26
14	21.5
14	27.5
15	24.5
15	20.5
16	27
Average	25.1 ± 2.6

1.2 Laramide basement tectonics

One of the most controversial and least understood mountain forming styles is that of the Laramide orogeny (40-70 Ma) in the central and southern Rocky Mountains of the United States. The basement block, "germanotype", or "thick-skinned" tectonic style of the Laramide orogeny is characterized by broad zones of uniform strike and dip separated by narrow zones of steeper dips or high angle faults. The overlying sediments may be folded or "draped" over the faulted basement blocks forming monoclines. Bouguer gravity anomalies directly reflect the movement of the basement blocks. The uplifts have

Bouguer gravity anomaly highs indicating that dense basement rocks are involved and that the uplifts are "rootless", i.e., without crustal thickening.

A controversial question has been whether the basement uplifts were formed by compressional tectonics or by vertical tectonics (Figure 1.5, Miller and Mitra, 2011). Proponents of vertical tectonics believe that the magnitude of the vertical displacements exceeded the magnitude of horizontal displacements during the Laramide orogeny (e.g., Stearns, 1975). Subsequent seismic studies have revealed significant crustal shortening by brittle thrust faulting (e.g., Smithson et al.; 1979, Erslev, 2013).

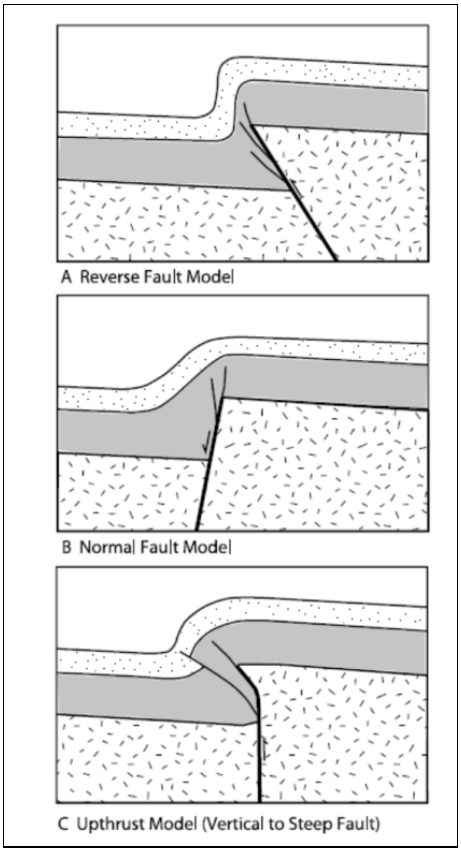

Figure 1.5: Models proposed for basement uplifts (Miller and Mitra, 2011)

A typical uplift bounding structure is the Casper Arch Thrust Fault (Figure 1.6, Skeen & Ray, 1983). Interpretation of seismic data indicates that the horizontal displacement on the Casper Arch thrust decreases from north to south with the fault angle increasing from 20 degrees in the north to nearly 40 degrees in the south. A sliver of overturned Paleozoic and Mesozoic rocks is present beneath the Precambrian thrust.

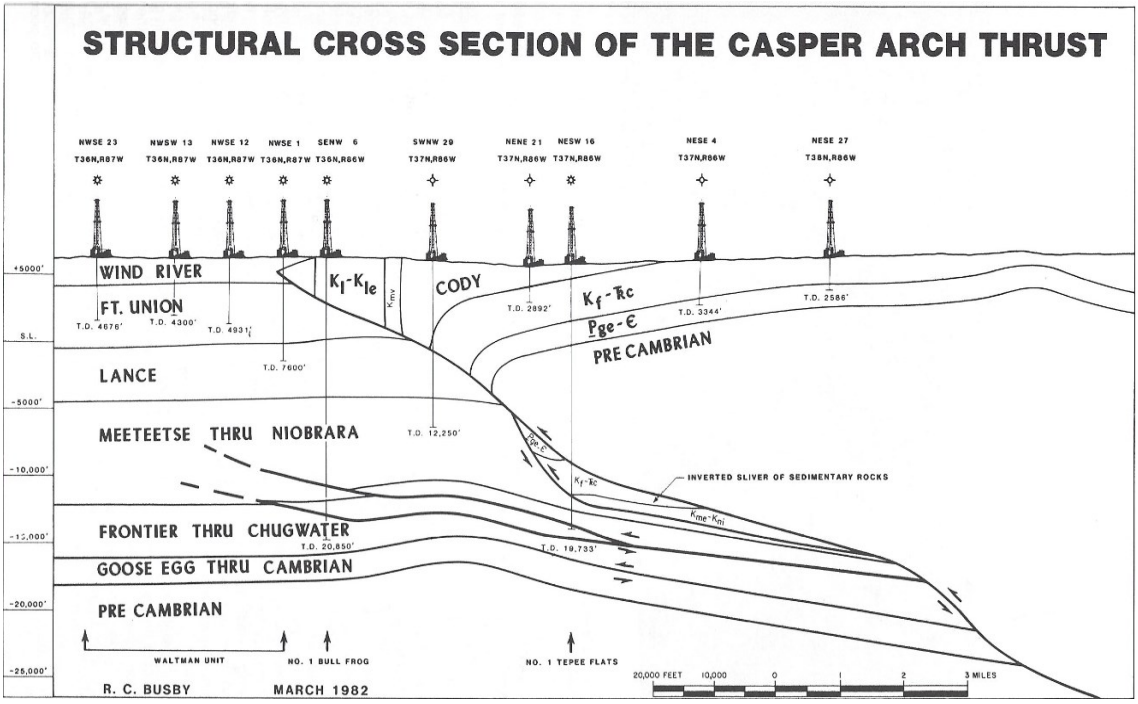

Figure 1.6: Cross section of the Casper Arch thrust fault (Skeen & Ray, 1983)

The common occurrence of overturned fault slivers of Mesozoic or Paleozoic sediments beneath the Precambrian rock hanging wall thrusts suggest a fault-related folding kinematic model for many of the Rocky Mountain basement uplifts. Low-temperature, basement-involved compressive folds are confined largely to the hanging walls of thrust faults and appear to be produced in response to both propagation and slip on non-planar faults. Kinematic models of three Laramide structures, including the Big

Thompson anticline, Colorado (Figure 1.7) by Narr and Suppe (1994) involve thrust faults propagating through the brittle upper crust along non-planar paths. The stratified cover sequence in many cases forms a drape fold or monocline over the propagating basement fault.

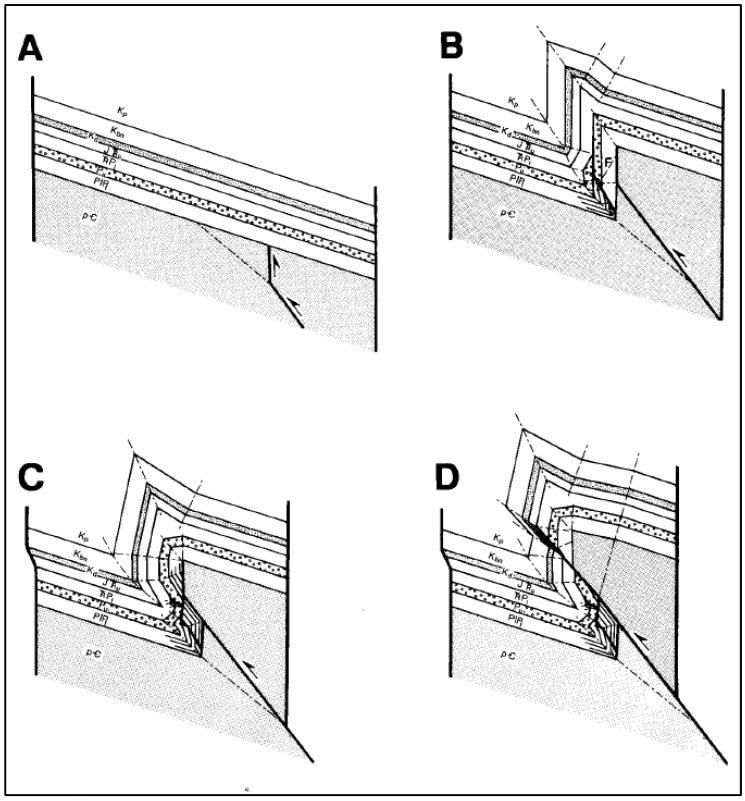

Figure 1.7: Cross sections showing the kinematic sequence of development of Big Thompson anticline Colorado (Narr and Suppe, 1994)

As of 1983, 16 wells had been drilled through Precambrian rocks for oil and gas prospecting in the sedimentary rocks that are concealed and virtually unexplored beneath the Rocky Mountain – front thrusts (Gries, 1983). The wells set up an exciting play and helped define the structural geometry of the mountain-front thrusts, including the angle of the thrust, the amount of horizontal displacement, and the presence or absence of fault

slivers containing overturned Mesozoic or Paleozoic rocks. Table 1.2 lists the well depths, dips of the fault angles at TD, and subthrust fault sliver thicknesses, if available.

Table 1.2: Well Data of Gries (1983) compared to Iskana – 1 (Garzón Fault) showing dip angles at TD (Total Depth). Only wells with known dips at TD are included.

Well Name and Operator	Thrust	TD (m)	Dip at TD	Subthrust fault sliver thickness (m)
Carter 1 Unit	Emigrant Trail	2009	13.0	268
Shell 1 Govt.	E A	3258	15.0	250
Sinclair 1 Cooper Creek	Emigrant Trail	1997	20.0	none
Mountain Fuel 1 Dickey Springs	Wind River	5212	8.5	none
American Quasar 1 Skinner Fed.	Uinta Mountain	4584	50.0	1189
Champlin Fed. 31 - 19 (Bear Springs)	Uinta Mountain	4209	15.0	none
West Coast Oil 1 Skinner Fed.	Wind River	2468	45.0	unknown
Mobil C – 1 McCormick Fed.	Uncompahgre	5873	27.0	unknown
Supron Energy 1 F - 28 - 30 - 93	Emigrant Trail	2368	10.0	137
ISKANA 1A	**Garzón Fault**	**1164**	**17.0**	**none**

Number of Data	10.0
Mean	22.1
Standard Deviation	14.4

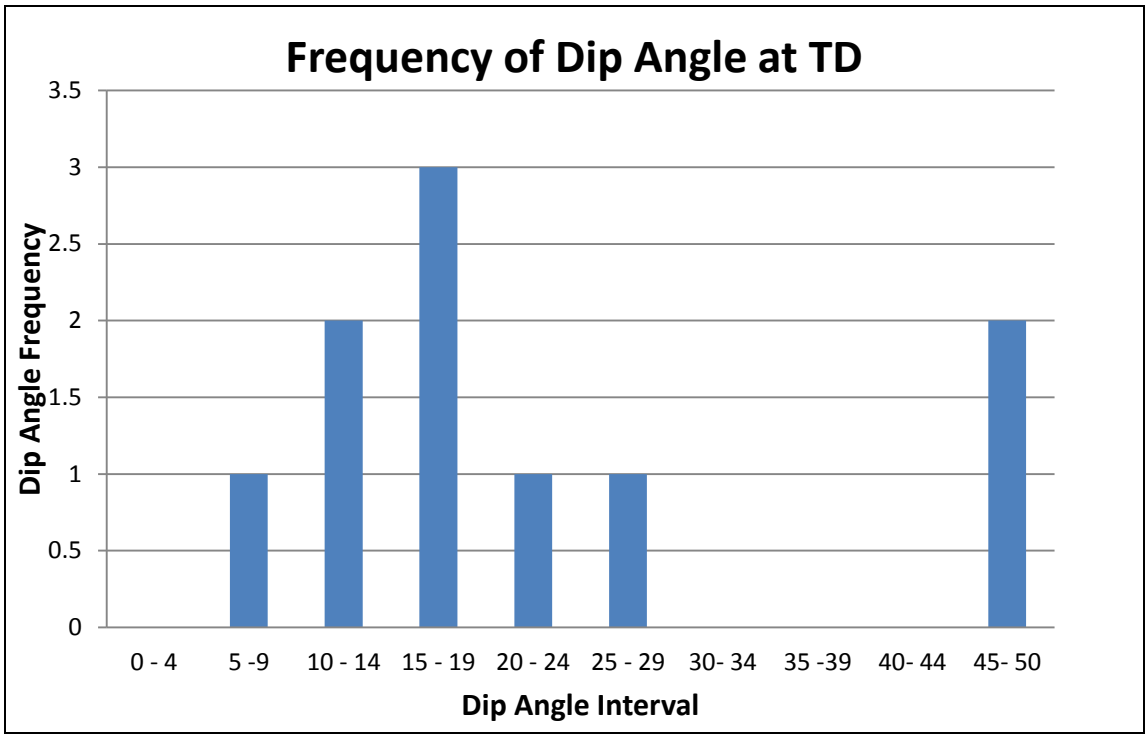

Chart 1.1: Frequency of Dip Angle at TD (Total Depth).

The mean dip angle from the ten wells is 22° with a large standard deviation. As Chart 1.1 shows, the measured dip angle distribution is bimodal, but the most common mode is low angle thrusting (5 to 30 degrees). The measured Garzón thrust well dip angle (17°) lies in the middle of the most common thrust mode.

1.3 Laramide-style faulting in the lower crust

Geophysical data, primarily seismic and gravity have shed light on Laramide-style deformation in the lower crust. Deep seismic reflection profiles across the Wind River Mountains, the largest Laramide uplift, show reflections from the a thrust fault flanking the Wind River uplift to at least 24-km depth and possibly as deep as 36 km with a fairly uniform dip of 30° to 35° (Figure 1.8, Smithson et al., 1987). There is at least 21 km of crustal shortening along the thrust. The seismic results confirmed previous predictions based on gravity models. The gravity data suggests that the fault does not displace the Moho.

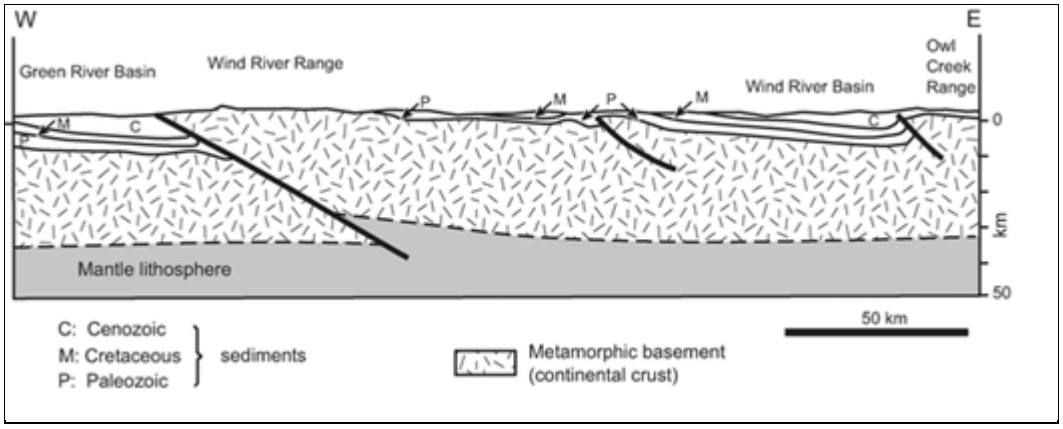

Figure 1.8: Cross section of the Wind River Mountain showing the Wind River thrust fault. Note that seismic and gravity do not support offset of the Moho.

Passive source crustal imaging of the Bighorn Arch Seismic Experiment (BASE) and EarthScope USArray Transportable Array show that the crust thins under the Bighorn Arch with no apparent crustal root or major fault offsets (Figure 1.9, Worthington et al.,

2012; Yeck et al., 2013). The Bighorn Arch master thrust rooted in a lower crustal detachment at ~ 30 km depth (Erslev, 2013).

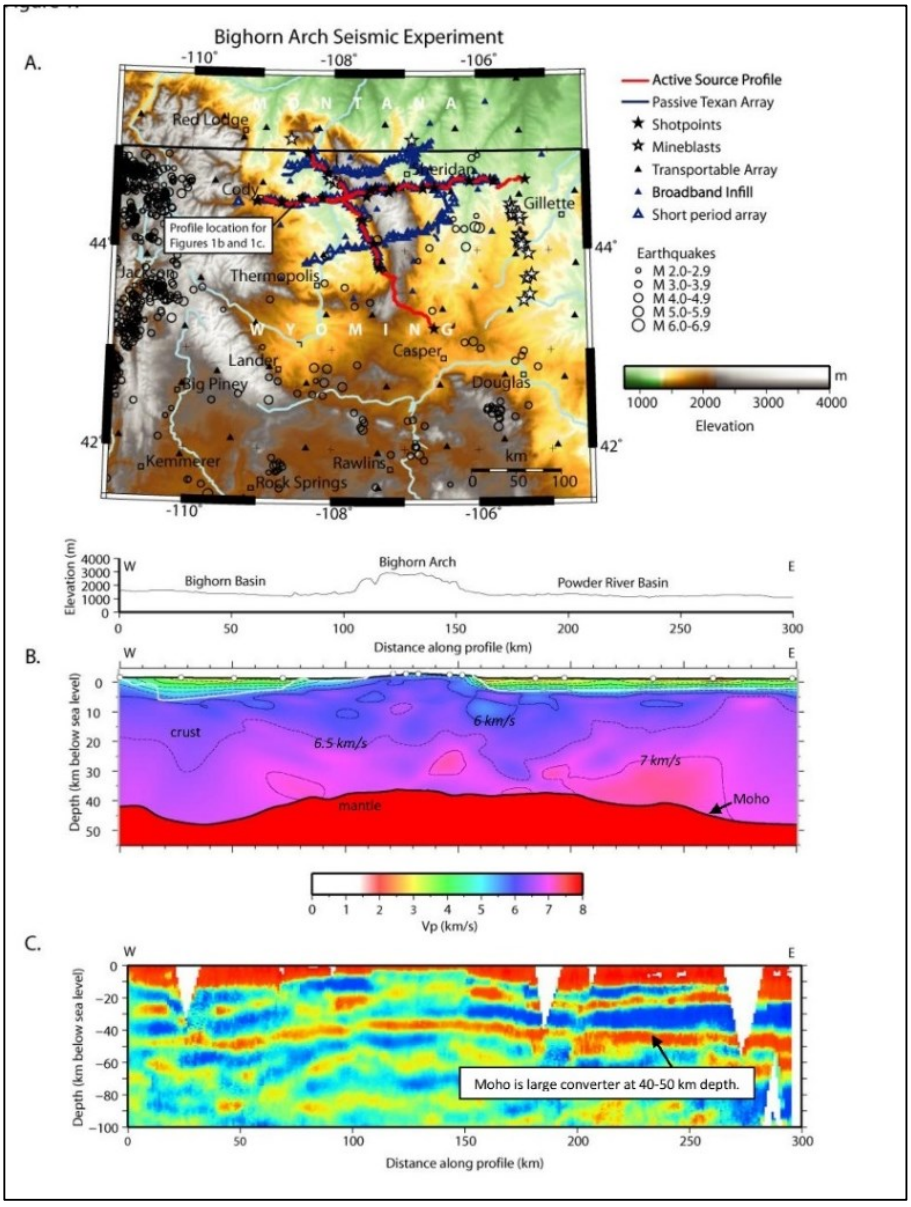

Figure 1.9: A) Study area and survey geometry for Bighorn Arch Seismic Experiment; Elevation profile across east – west seismic line shown in Figures 1B and 1C. B) Seismic P –Wave velocity model across Bighorn Arch derived from tomographic inversion of travel – time data. C) Common conversion point (CCP) stack of teleseismic receiver functions. (Worthington et al. 2012)

CHAPTER 2: LOCATION & GEOLOGIC BACKGROUND

The study area is located in the southeastern Colombian Andes. The Garzón Massif is the southern extension of the Eastern Cordillera. The Garzón Massif is an uplifted basement block bounded by the Upper Magdalena Valley to the northwest and the Llanos to the southeast (1.7 – 2.5^{O} N, 75 – 76^{O} W) (Figure 2.1). The Garzón Group consists of 1.2 – 1.0 Ga old granulites, gneisses, amphibolites and minor ultramafic and calcsilicate rocks.

The Pacific margin of the northern Andes was formed during the breakup of Rodinia. Some of the terranes comprising the northern Andes are left from the breakup of Rodinia on the western Gondwana margin whereas others are the results of Neogene collisions.

Geochronological studies indicate that the Grenville basement ages on the terranes forming the northwest margin of South America were correlated with the amalgamation of Rodinia, included the Andaqui terrane exposed in the present Garzón Massif. According to Van der Wiel's (1991) geochronological studies, the major uplift events in the Garzón Massif from 1.18 Ga to the present day are:

(I) 1180 Ma: Relative uplift of 6 km.

(II) 900 Ma: An orogeny, possibly related to Grenville, resulted in at least 10 km uplift.

(III) 12 Ma: 6.5 km of uplift related to the Panama Arc Collision.

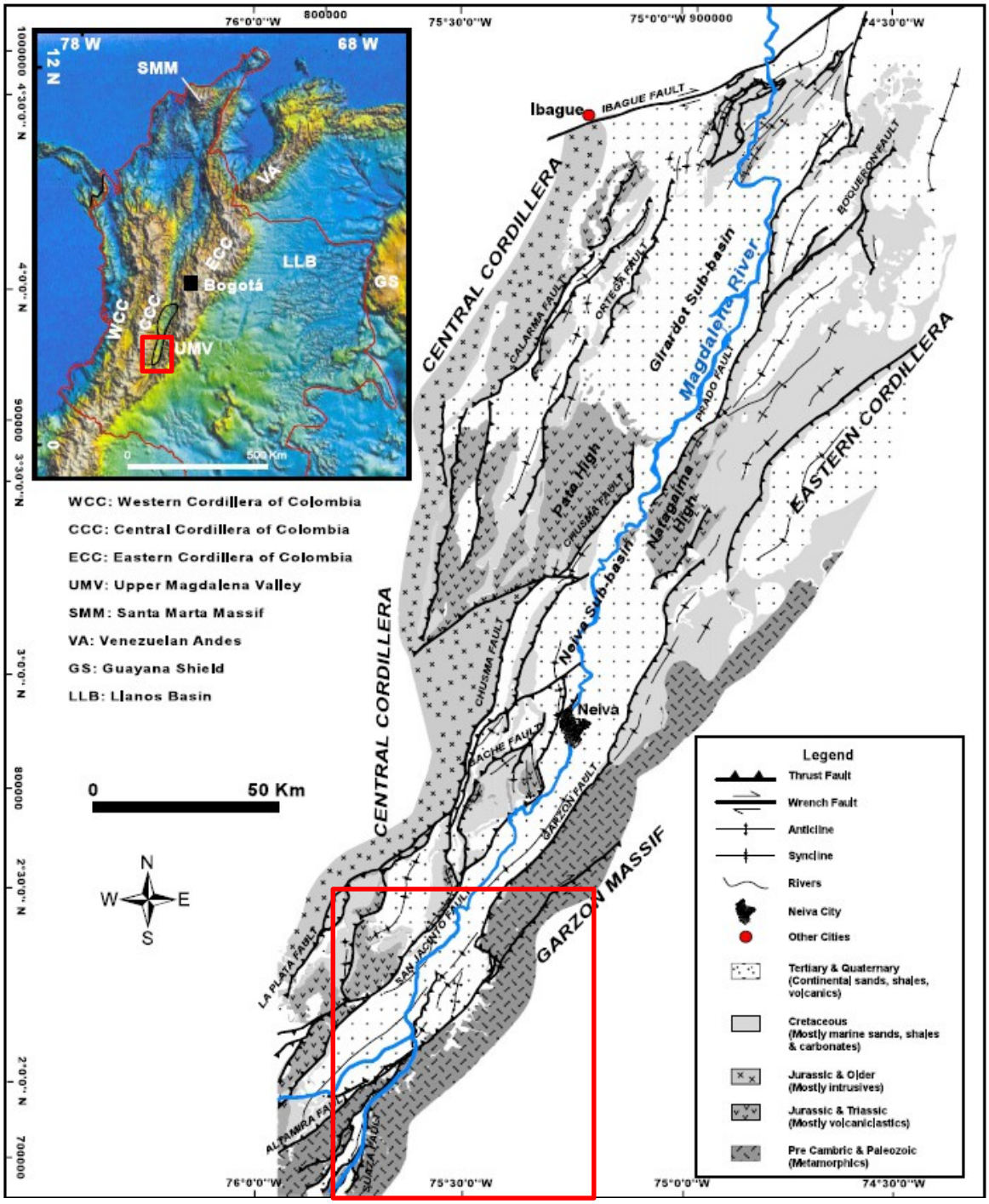

Figure 2.1: Location and simplified geologic map of the Upper Magdalena Valley, Colombia. (E.Jaimes, 2004)

CHAPTER 3: METHOD OF INVESTIGATION

Velocity-Depth Model: An initial depth model was derived from well logs, the unmigrated seismic reflection profile, and a down-hole velocity survey. The model included depths to the Garzón thrust fault, the top of Barzalosa Fm, and the top of Saldaña Formation (basement). The initial model correlates well with the migrated seismic profile. However, the dip of the Garzón fault is ambiguous to the southeast of the well data; hence, the value of an independent dip estimate from gravity data.

Gravity Map: Airborne gravity data were used to produce a Bouguer Anomaly Gravity Map and input to Geosoft Oasis Montaj gravity modeling software. Observed gravity was then extracted from the data along the profile line.

Rock Densities: Average rock densities were estimated from well density logs, seismic velocities, and formation rock types.

Regional Gravity Field: The regional gravity field was estimated from the profile to the northwest of the Garzón fault, where the sedimentary section is well imaged seismically and constrained by the Gigante-1 well. The regional was successfully modelled by dense lower crustal basement and mantle shallowing to the southeast under the Garzón Massif.

2-D Density Models: 2-dimensional forward models were then constructed with average well densities, seismic velocities, and rock types, and the initial depth model from well and seismic data west-northwest of the Garzón fault. The calculated model gravity fit the observed gravity remarkably well west-northwest of the Garzón fault. Then, using the best density estimate for the Garzón Massif, the model dip on the Garzón fault was varied to produce the best fit between the calculated and observed gravity anomalies. Since the model fit is dependent on the density assumed for the Garzón Massif rocks, multiple densities and dip angles were tested, and the errors between calculated and observed are compared for 11 densities and 8 dip angles.

Magnetic Maps & 3D Euler Deconvolution: Magnetic map and inversion were generated with the various aeromagnetic airborne surveys acquired from Agencia Nacional de Hidrocarburos, the National Colombian Hydrocarbon Agency. The airborne magnetic data are used to produce a Magnetic Anomaly Map for the regional profile and inverted using Euler Deconvolution Geosoft modelling software. The magnetic inversion highlighted fault boundaries and contacts within the crystalline basement rocks.

Regional Profile: A schematic regional profile across the entire Garzón Massif was constructed using surface geology maps from Ingeominas, constrained with aerogravity and aeromagnetic data and seismic data from Block VSM – 32. The regional profile tested whether the uplift was symmetric or asymmetric, the extent of basement involvement, and the depth of the Garzón Fault.

Retrodeformed Model: The regional model was retrodeformed to 25 Ma with Midland Valley MOVE structural software to estimate the total uplift and horizontal shortening.

CHAPTER 4: GEOPHYSICAL STUDY OF THE GARZÓN BASEMENT TECTONICS

The geophysical study focused on the interpretation of the Garzón fault with two dimensional gravity forward modeling constrained by seismic and well data. Then, a regional 2D model of the entire Garzón Massif based on surface geology, gravity and magnetic data was developed. The model was then retrodeformed to 25 Ma to interpret the orogenic evolution of the mountain. The magnetic field was also inverted with the Euler Deconvolution method to illuminate lateral variations in the PreCambrian basement rocks of the Garzón Massif.

4.1 Density Models for the Geometry of the Garzón Fault

4.1.1 Complete Bouguer Gravity Anomaly Map (g = 2.8 g/cm^3)

The airborne gravity survey data used in the project includes 2,663 line kilometers gravimetry along 1 x 5 and 1 x 4 kilometer flight lines at elevations of 2564 and 4589 meters above mean sea level (Figure 4.1). The data were obtained from the Agencia Nacional de Hidrocarburos Gravity Map of Colombia (Graterol, 2010). ArcGIS was used to create shapefiles and raster files from the database created in Oasis montaj. Moreover, the elevation and gravity raster gridded maps were converted to raster files in ArcGIS

10.1. The Bouguer gravity map was generated using a 0.5 x 0.5 kilometer grid generated by the Geosoft Oasis Montaj graphic mapping system (Figure 4.2). Figure 4.2 is the complete (terrain corrected) Bouguer gravity map calculated for a reduction density of 2.80 gr/cm^3. The Bouguer map is constructed by upward continuing the low elevation data (2564 meters above sea level) and merging it with the high elevation data (4589 meters above sea level). The accuracy of the airborne gravity observations are confirmed by land gravity observations collected along a north south profile east of the Iskana-1 well, in addition to land observations to the west of line GAIT 99-21. Misfits between land and air gravity measurements are less than 3 mgal. The observed gravity was then extracted from the map data grid along the GAIT 99-21 profile line and exported to the 2-D profile. The range of the observed gravity is from -156 mgal to -84 mgal.

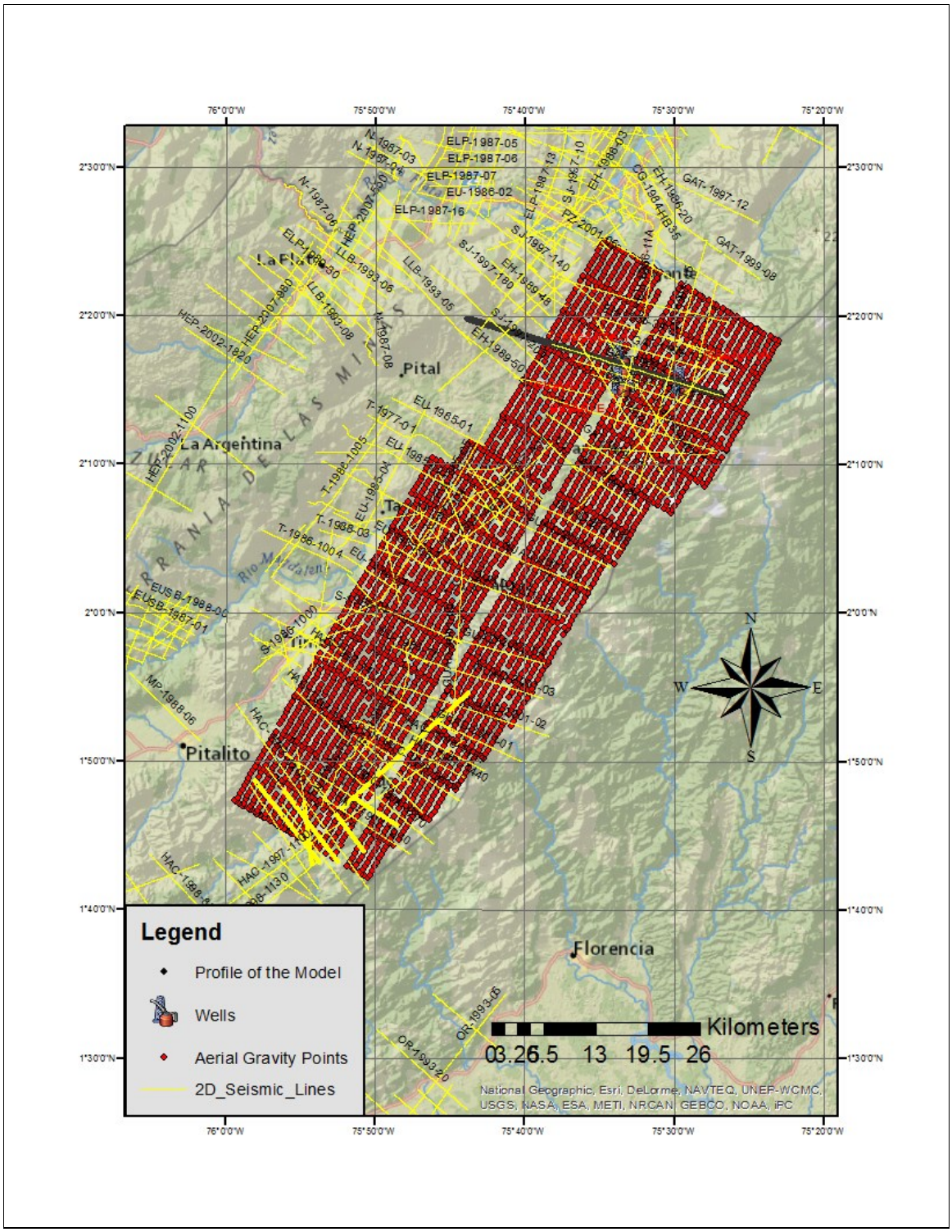

Figure 4.1: Location map for airborne gravity and magnetic survey of Block VSM – 32

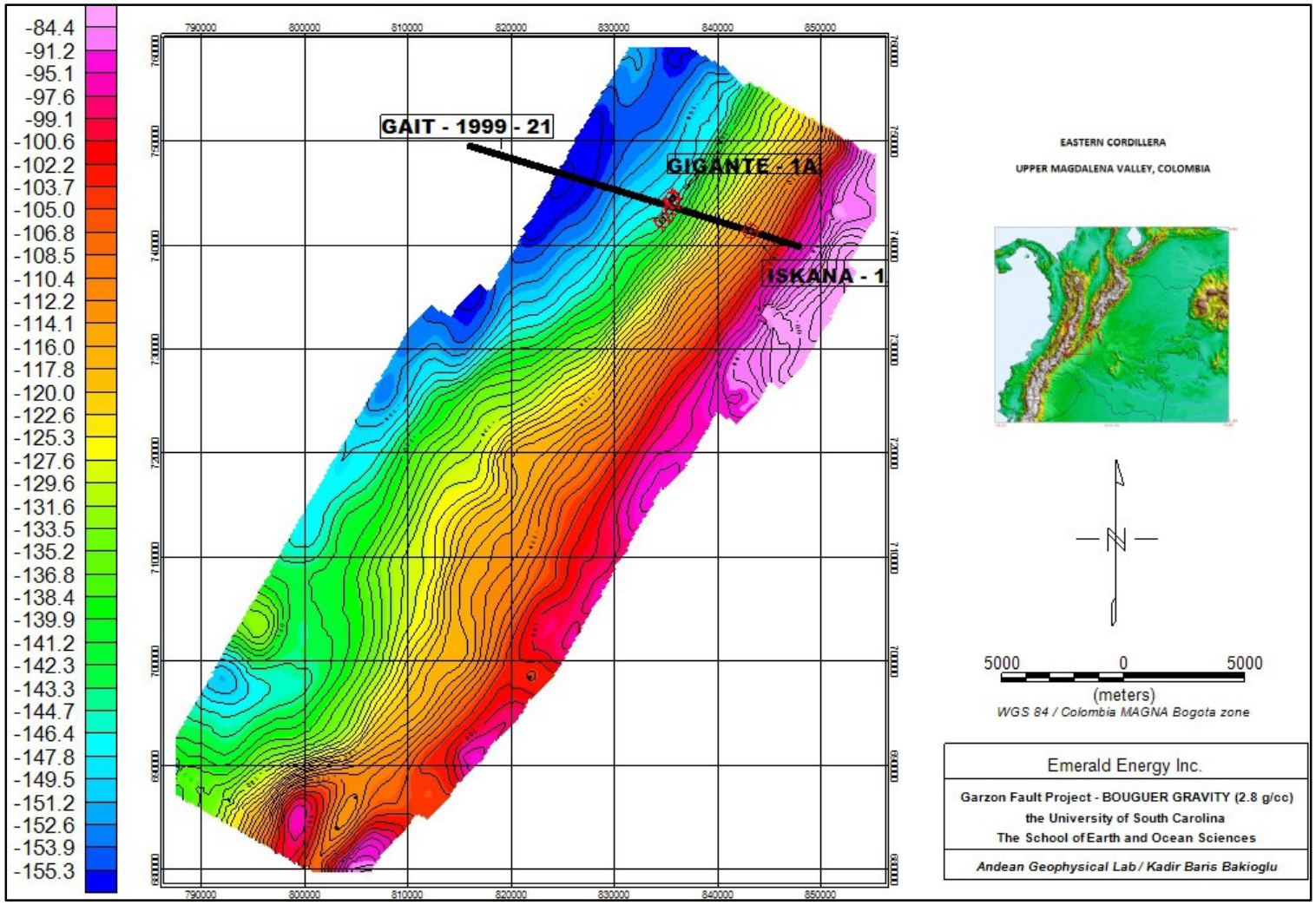

Figure 4.2: Complete Bouguer Gravity anomaly map with the reduction density of 2.8 g/cm^3. Map area is approximately the same as Figure 4.1.

4.1.2 Velocity – Depth Model

An initial depth model for line GAIT 99-21 was derived from the Iskana-1 and Gigante-1 well logs, the unmigrated seismic reflection profile, and the down-hole velocity survey for Iskana-1. The model included depths to the Garzón thrust fault (northwest of Iskana-1), the top of Barzalosa Fm, and the top of Saldaña Formation (basement). The initial model correlates well with the migrated seismic profile provided by Emerald. However, the dip of the Garzón fault is ambiguous to the southeast of the Iskana-1 well; hence, the value of an independent dip estimate from gravity data.

4.1.2.1 Well Control

The Iskana-1 and Gigante-1 well logs, the unmigrated seismic reflection profile, and the downhole velocity survey for Iskana-1 were used to produce an initial depth model for line GAIT 99-21. The seismic profile is fairly unambiguous so it relatively straightforward to make the time-depth conversion.

The Iskana-1 and Gigante-1 wells were located on the profile. Downhole deviations are not shown, but were accounted for in the depth model. Depths to tops of formations are as reported by Emerald (Table 4.1). The surface fault trace of the Garzón fault was located from surface geology (Tapias, 2007, referred to as Algeciras fault) and from the clear fault impedence contrast in the migrated seismic image (Figure 4.3 and 4.4).

Table 4.1: Well depths to formation tops.

	ISKANA - 1A (MSL)		GIGANTE - 1A (MSL)	
FORMATIONS	**Depth (m)**	**Depth(ft)**	**Depth (m)**	**Depth (ft)**
HONDA FM	1151	3777	-	-
BARSALOZA FM	1539	5050	578	1895
GUADUALA FM	2729	8952	2252	7388
VILLETA FM	3276	10747	2994	9823
CABALLOS FM	3610	11844	3603	11820
SALDANA FM	3613	11854	3683	12082

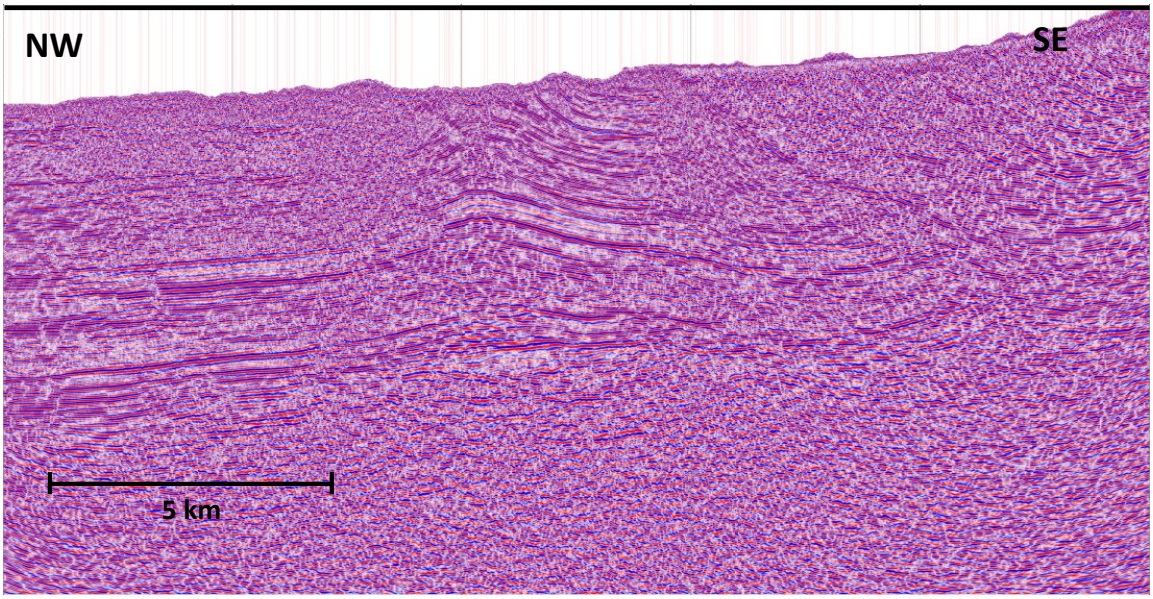

Figure 4.3: Migrated seismic line GAIT – 99 – 21. See figure 4.1 and 4.2 for the location (Vertical Exaggeration: 1)

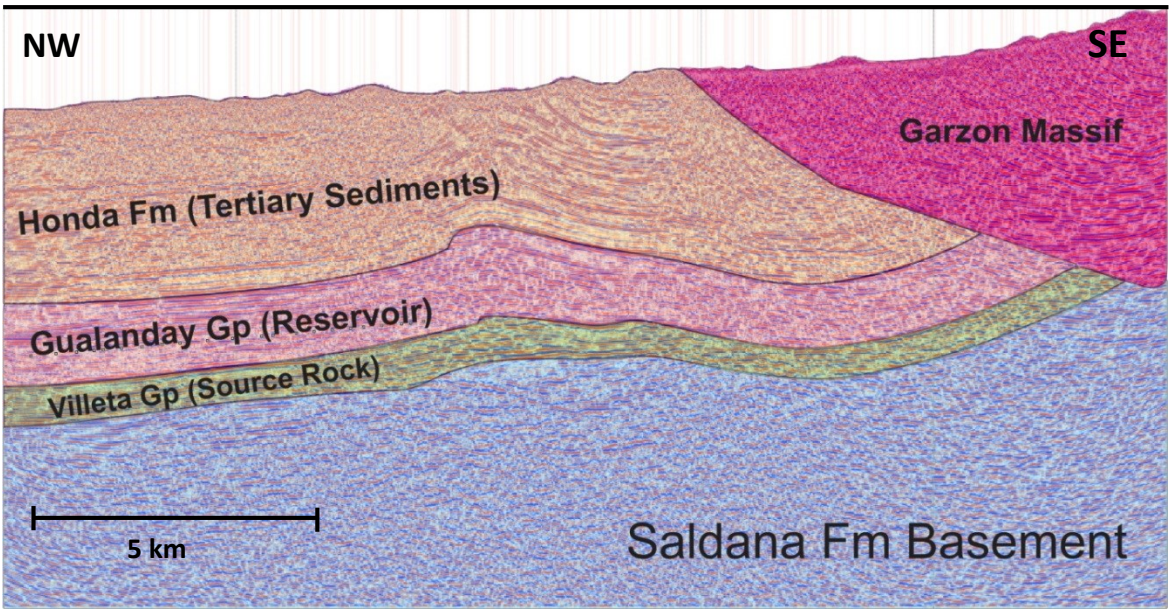

Figure 4.4: Interpretation of Migrated seismic line GAIT – 99 – 21 (Vertical Exaggeration: 1).

Honda Formation: Well velocity logs for Gigante-1 indicate an average of approximately 11,600 feet/sec. (3.53 km/sec) for the Honda Formation (Figure 4.5).

Barzalosa Formation to Caballos Formation: Well logs (Figure 4.5) indicate an average velocity of approximately 14,500 feet/sec. (4.11km/sec) for the pre-Honda sedimentary section (Barzaloza Formation to Caballos Formation).

Saldaña Formation (Basement): The top of basement (Saldaña Formation) was penetrated by both the Gigante-1 (referred to as Motema Formation) and Iskana-1 wells. The velocity in Gigante-1 well rocks at the bottom of the well averaged 16,500 feet/sec (5.03 km/sec).

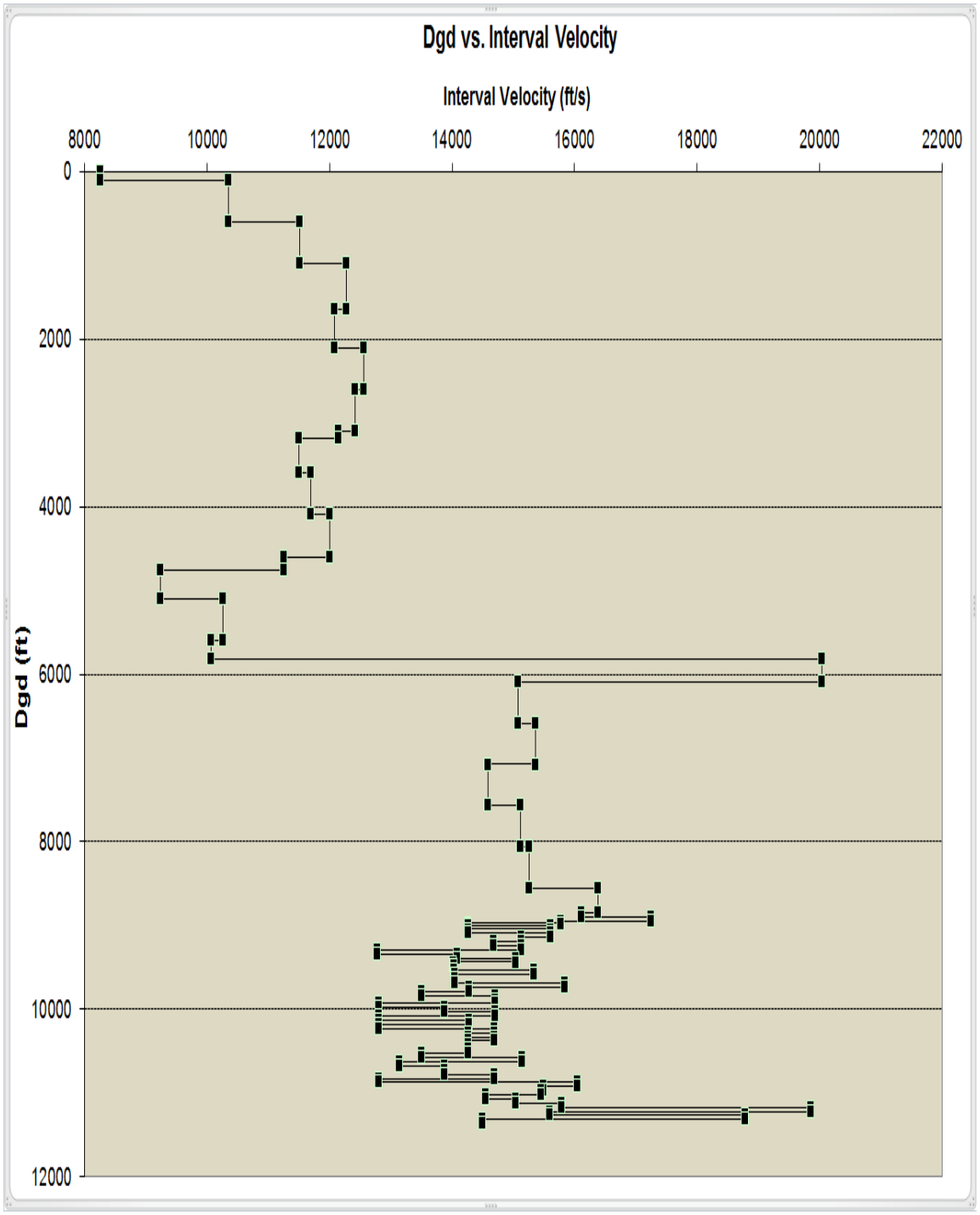

Figure 4.5: Gigante – 1 interval velocities.

4.1.2.2 Seismic Depth Model

Using seismic velocities from Gigante-1, the unmigrated seismic profile GAIT 99-21 (Figure 4.6) was used to produce an initial depth model (Figure 4.7).

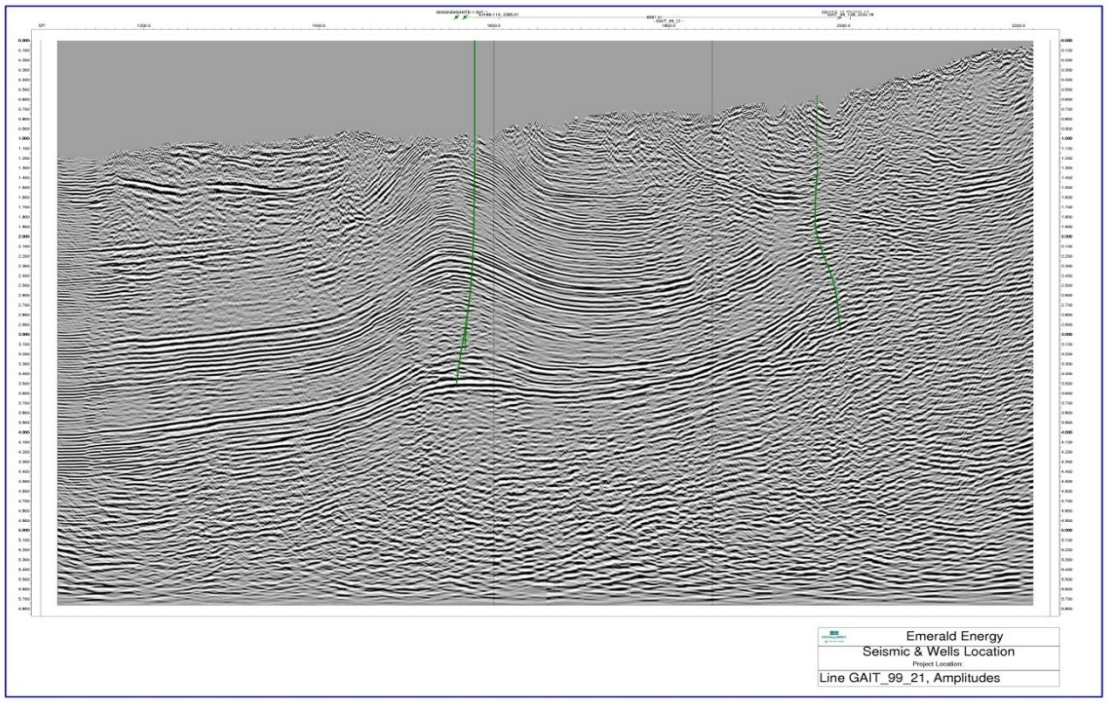

Figure 4.6: Unmigrated seismic line GAIT – 99 – 21 showing well derivations.

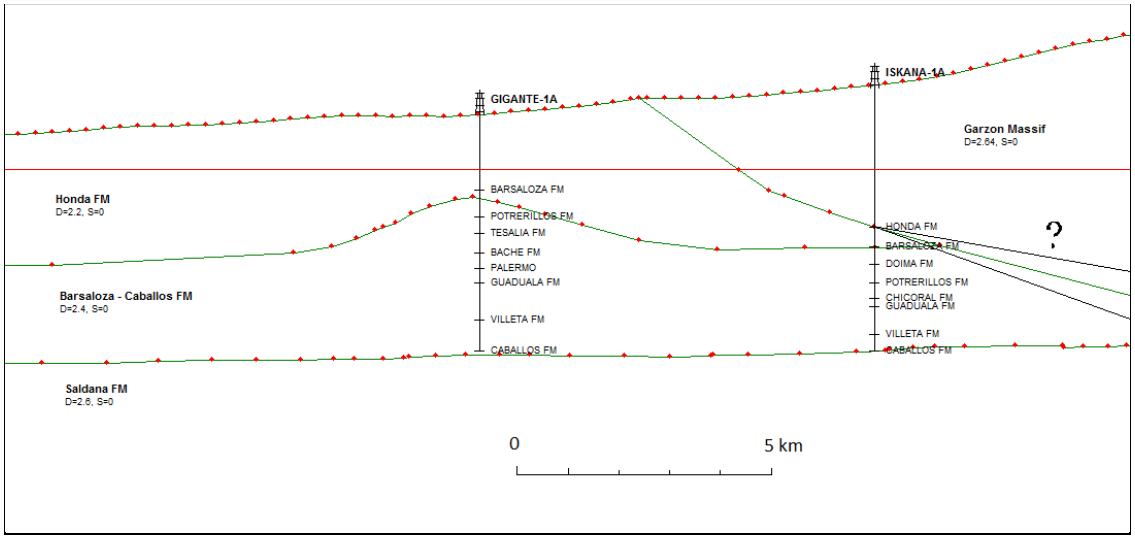

Figure 4.7: Seismic depth model (GAIT – 99 – 21). Red line is sea level. No vertical exaggeration.

i. Barzalosa Formation

In our depth model (Figure 4.7) the top of Barzalosa Fm. is located at a depth of 1887 meters (6,226 feet) below sea level on the northwest end of the seismic line, shallowing southeastward to Iskana-1 well where it is at a depth of 1539 meters (5,050 feet) below sea level. In Gigante-1 anticline the top of Barzalosa Fm. was reported at a depth of 411 meters or 1350 feet below sea level.

ii. Saldaña Formation (Basement)

The top of the Saldaña Formation (Basement) gradually shallows southeastward from 3844 meters (12,611 feet) below sea level to 12,082 feet (Motema Fm) in Gigante-1, 11,854 feet in Iskana-1, and 3475 meters (11,469 feet) below sea level at the southeast end of the seismic profile.

iii. Garzón Fault.

With the surface fault trace known and the depth of the Garzón fault in Iskana-1 well, the dip of the Garzón thrust fault to the northwest (updip) of Iskana-1 can be estimated with high reliability. The form of the fault (Figure 4.7) is a listric thrust dipping 33 degrees (apparent) to the southeast near the surface. At a depth of 420 meters (1379 feet) below sea level, the apparent fault dip shallows to 19 degrees southeast until it is intersected by Iskana-1 well. Dipmeter and VSP independently suggest a fault dip of approximately 17 degrees. Taking into account the obliquity of the profile relative to the trace of the Garzón fault, the true dip of the fault is approximately 35 degrees southeast at the surface, shallowing to 21 degrees at a depth of 420 meters below sea level. Overall,

the initial depth model (Figure 4.7) correlates well with the migrated seismic profile (Figure 4.3). However, the dip of the Garzón fault is ambiguous in the seismic data to the southeast of the Iskana-1 well. The uncertain location of the fault southeast of the Iskana-1 well was the impetus for this project to develop an independent dip estimate constrained by observed gravity data.

4.1.3 Regional Gravity Model

Since the primary goal of this project was to interpret the geometry of the Garzón fault and the secondary goal is to interpret depth to basement, the long-wavelength "regional" gravity signal produced in the lower crust or mantle must be first quantified. Along the northwestern half of profile GAIT 99-21 the "regional" gravity not explained by the sedimentary section above basement increases to the southeast toward the Garzón Massif. The regional gradient (Figure 4.8) can be defined by shallowing of the dense lower crust (2.7 to 2.8 gr/cm^3) and mantle (3.2 gr/cm^3) toward the southeast under the Garzón Massif.

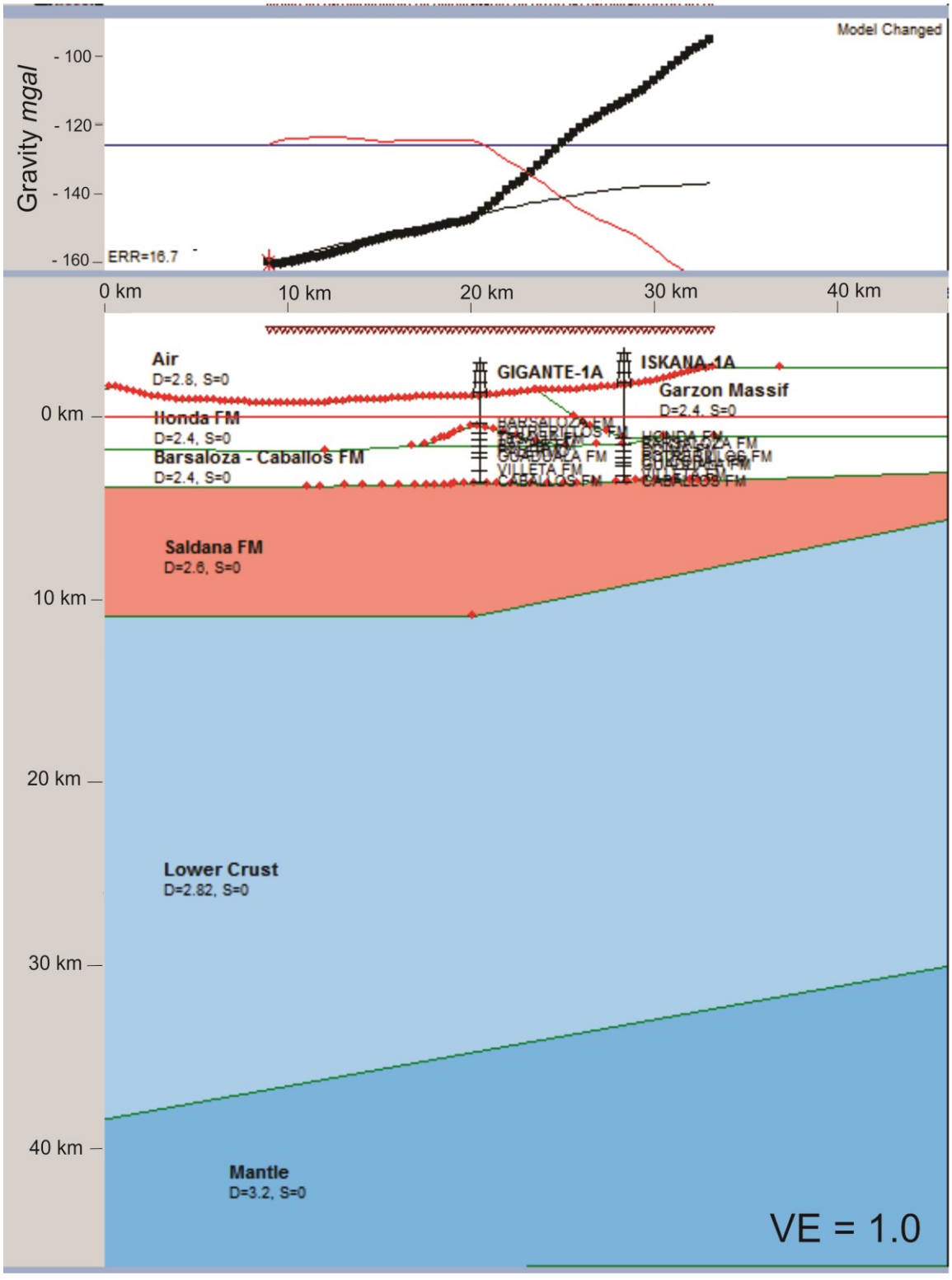

Figure 4.8: Regional gravity gradient explained by shallowing of the dense lower crust and mantle to the southeast (right).

4.1.4 2D Density Models of GAIT – 99 – 21

i. Rock densities

Honda Formation: The density used in the models for the Honda Formation is 2.2 gr/cm^3 (Table 4.2). This density is typical for claystones and siltstones, and matches the well average bulk densities in the upper 6,000 feet of Gigante-1 well. The density also corresponds well with the average seismic velocities of 11,600 feet/sec in the upper part of the well.

Table 4.2: Rock Density/velocity table.

FORMATIONS	VELOCITY (km/sec)	VELOCITY (ft/s)	DENSITY (gr/cm3)
HONDA FM	3.53	11600	2.2
BARSALOZA - CABALLOS FM	4.11	14500	2.4
SALDANA FM	5.03	16500	2.6
GARZÓN MASSIF	5.39	17678	2.64 (2.6 - 2.7)
LOWER CRUST	-	-	2.76
MANTLE	-	-	3.2

Barzalosa Formation to Cogollo Formation: Average bulk densities for the Lower Tertiary and Cretaceous rocks in Gigante-1 varied, but averaged 2.4 gr/cm^3 (Table 4.2). This density is typical for shales and sandstones (Telford, 1990). Seismic velocities averaged 14,500 feet/sec.

Saldaña Formation (Basement): An average density of 2.6 gr/cm^3 was assigned to the Saldaña Formation and basement rocks. Bulk densities of 2.5 gr/cm^3 and velocities of

16,500 feet/sec were recorded at the bottom of Gigante-1 well. Densities of rhyolites and quartzites vary between 2.5 and 2.7 gr/cm^3 and average 2.6 gr/cm^3 (Telford, 1990).

Garzón Massif: The Garzón crystalline rocks consist of PreCambrian age granites, granodiorites, and high grade quartzofeldspathic metamorphic rocks. Densities for these rock types can vary from 2.5 to 2.9 gr/cm^3. The average density for granites and schists is 2.64 grams/cc (Telford, 1990). Quartzites are 2.6 gr/cm^3, graywackes average 2.65, and granodiorites 2.73 gr/cm^3. Velocities in Iskana-1 well averaged 17, 680 feet/sec in the Garzón Massif above the Garzón thrust fault.

A density of 2.64 gr/cm^3 was determined to be the best average based on the rock types. However, since the model results vary with density selection, rock densities from 2.6 to 2.7 gr/cm^3 were tested.

4.1.5 Results

Northwest of Iskana-1 well, the profile geometries of the rock unit polygons determined from the well depth model were input as starting polygons for the density model (Figure 4.9). Initial rock densities were input from Table 4.2, based on rock type, bulk density logs from Gigante-1 well, and seismic velocities. WNW-dipping dense basement polygons were included for the lower crust and the mantle as shown in Figure 4.8 to explain the regional gravity gradient linearly increasing to the east-southeast. The air polygon was given a density of 2.8 grams/cc, since this is the reduction density used to produce the Bouguer anomalies. The resulting calculated gravity field for the 10 degree dipping fault model (Figure 4.9, solid line) agrees well with the observed gravity (dotted line). The only significant misfits are two observed gravity lows (3 mgal

amplitude, 2-3 km half-wavelength) over the Gigante-1 and Iskana-1A anticlines not fit by the model (positive errors shown by red line). These gravity lows may be produced by extensional fracturing in the folds or low density fluids. Determining whether these short wavelength gravity anomalies can be used as structural or hydrocarbon indicators will require further testing.

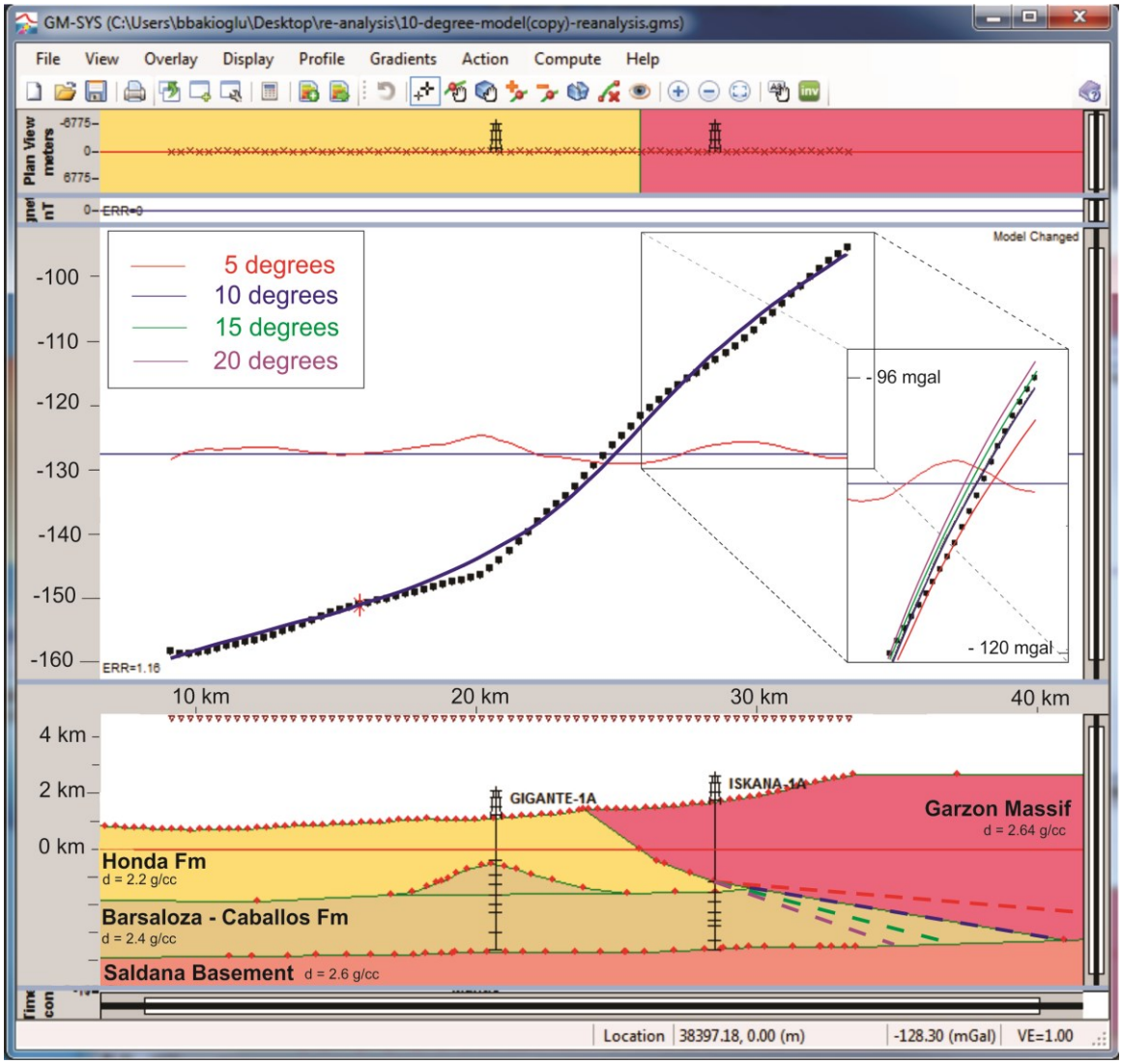

Figure 4.9: Density model for GAIT – 99 – 21. Model dips shown for Garzón thrust. Dips shown are 5, 10, 15, and 20 degrees. No vertical exaggeration. Calculated solid lines, observed dotted line, error red line (for 10 degree dip). Note the 2 positive errors (model gravity lows).

Since the model fit varies with the density chosen for the Garzón Massif polygon, the misfit errors were calculated for densities from 2.60 to 2.70 gr/cm^3 (Appendix A). Higher densities for the thrust, however, would indicate even shallower dips on the Garzón fault. The best fit model solutions are 10 to 15 degrees (12 to 17 degrees after correction for apparent dip because the profile is oblique to the maximum dip direction). This low angle thrust solution is supported by the measured 17 degree dip in the Iskana-1 well under the Garzón fault. It is also in agreement with the most common dip angles found for 10 exploration wells that drilled through Precambrian hanging wall blocks in the Laramide Rocky Mountains (Table 5; Gries, 1983).

4.2 Regional Structure and Geophysics Of the Garzón Massif

The second goal of this research project was to develop a geophysical and structural model to describe the tectonic evolution of the Garzón Massif. A regional cross section was constructed constrained by surface geology, gravity and magnetic data to quantify the horizontal shortening and uplift and to determine if the uplift was symmetrical. The regional profile geology was based on mapping by Ingeominas, the Colombian Geological Survey (Figures 4.10 and 4.11).

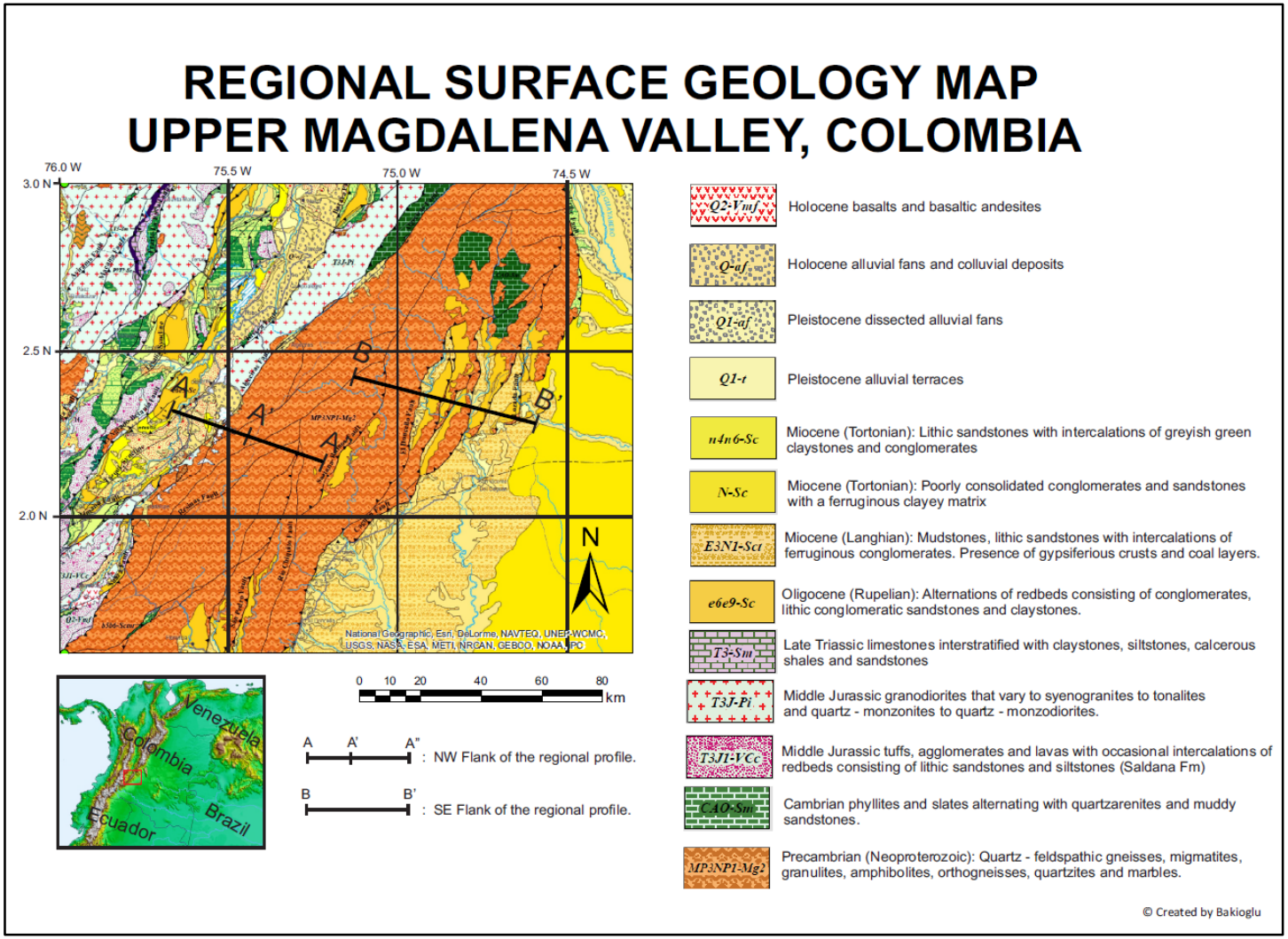

Figure 4.10: Regional geological map (Modified from Ingeominas, Geological Map of Colombia compiled by Tapias et al. 2007)

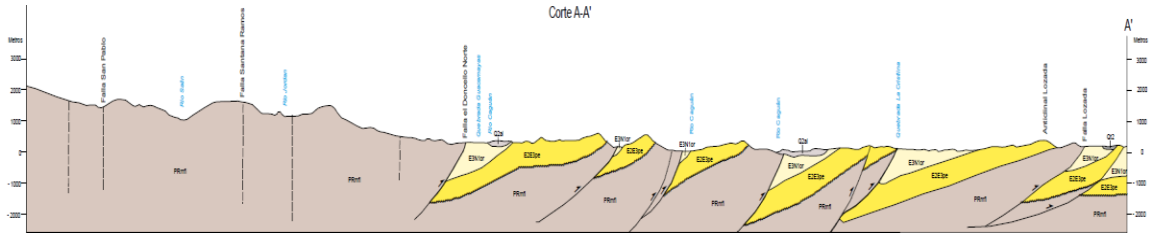

Figure 4.11: Cross section of Garzón Massif complex representing B – B' profile on regional map. Ingeominas Geología de la Plancha 368, San Vicente del Caguán. Escala 1:100.000. Mapa año 2003 versión digital 2010)

4.2.1 Geophysical interpretation of the Garzón Massif

Complete Bouguer anomaly and Total field and Reduced To Pole Magnetic anomaly maps (Figure 4.12, Figure 4.13 and Figure 4.14) were generated with data from Agencia Nacional de Hidrocarburos, Colombia. The gravity field of the northwestern flank of the Garzón Massif (Figure 4.12) is characterized by a steep NNE-SSW trending gradient. Southeastward from the high peaks of the Massif the gravity field extends with low relief toward the Llanos. The magnetic field (Figure 4.14) does not show a similar high correlation with the NW mountain front, and exhibits considerable relief over the basement rocks of the Massif. The magnetic field was inverted with Euler Deconvolution (structural index = 0) in Figure 4.14. The Euler solutions show several NNE-SSW trending patterns which are here interpreted as produced by faults bounding en-echelon grabens containing non-magnetic Precambrian sediments.

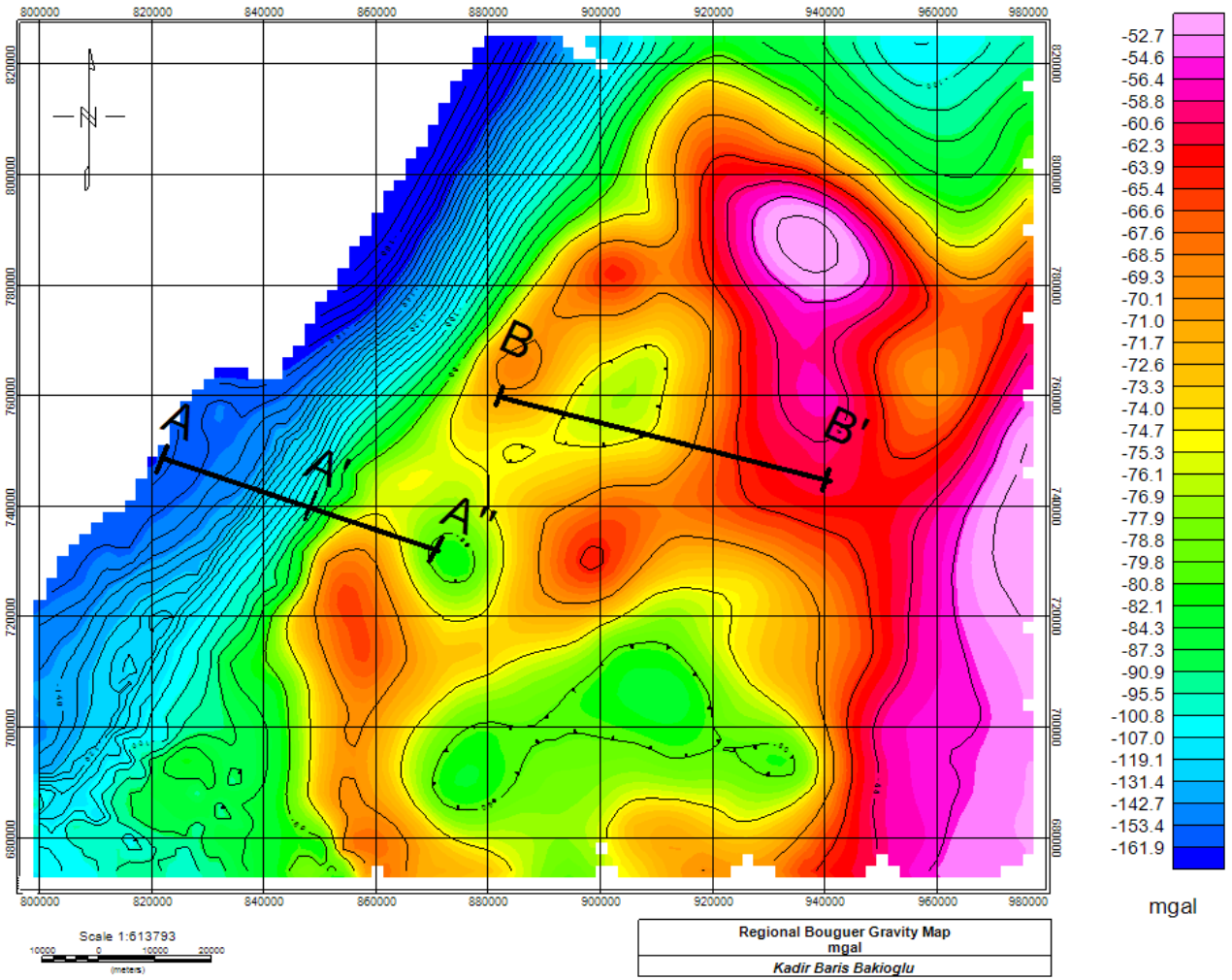

Figure 4.12: Regional Complete Bouguer Anomaly map projected with M AGNA – SIRGAS Colombia Bogota Zone coordinate system.

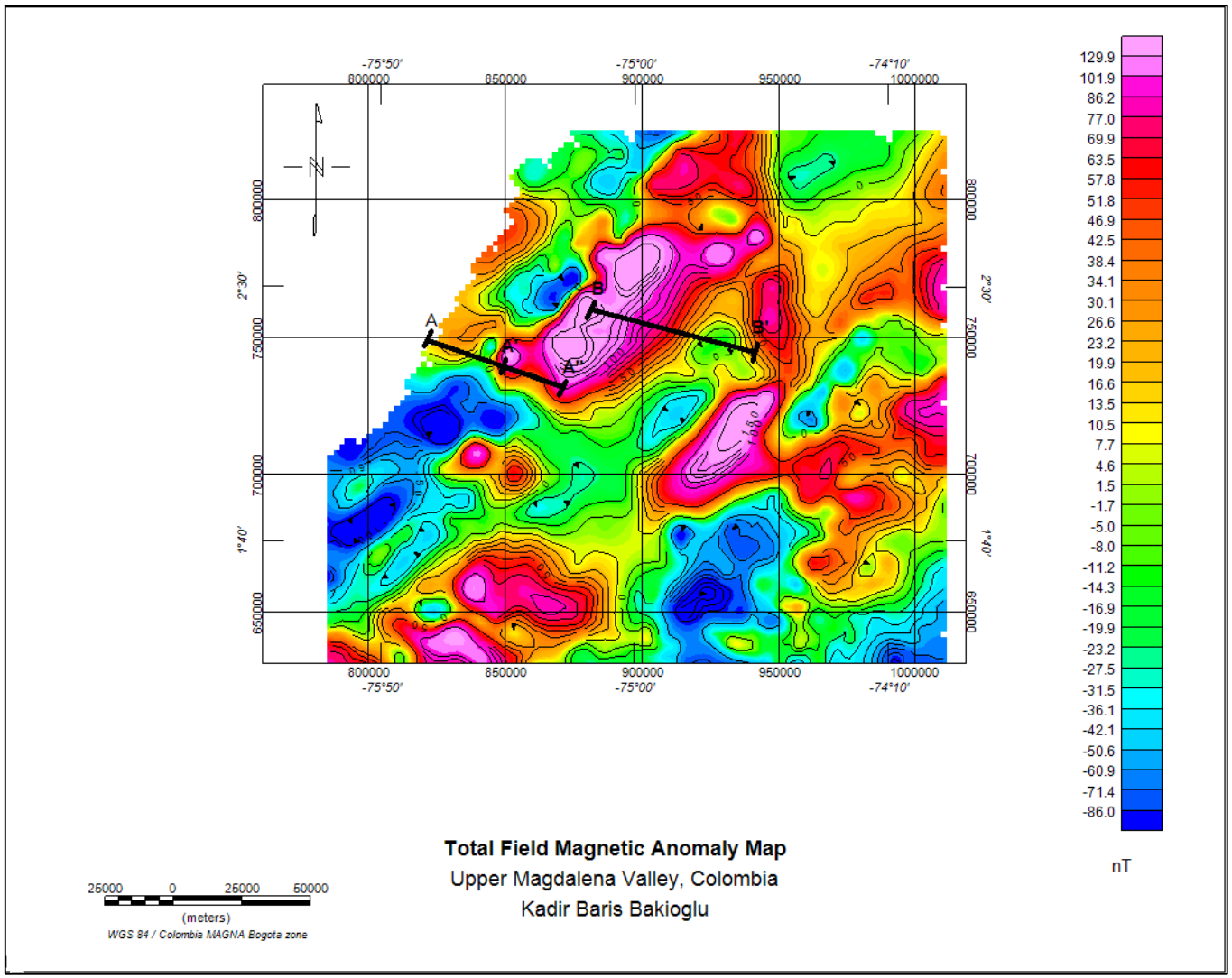

Figure 4.13: Total Magnetic Anomaly Map.

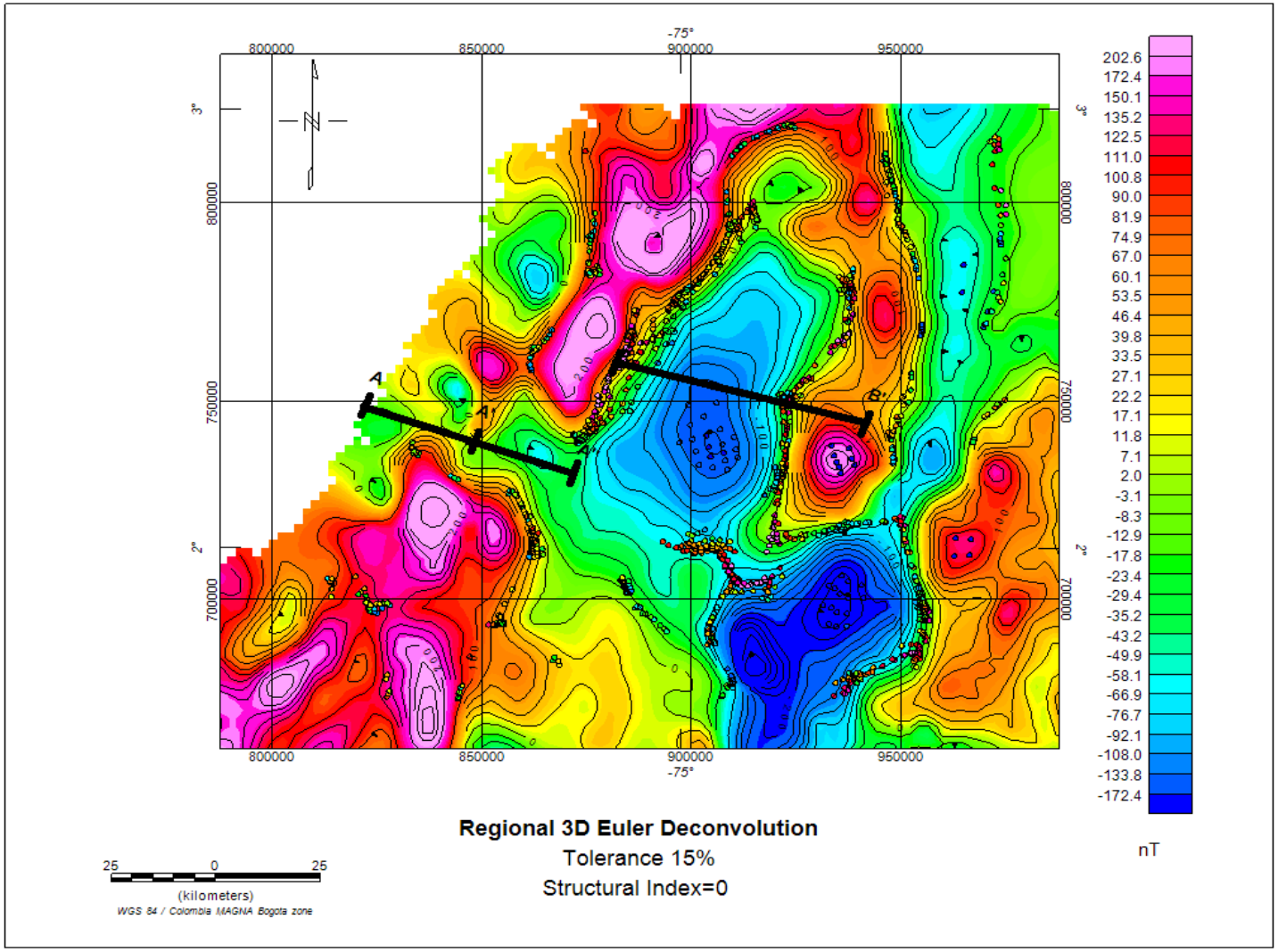

Figure 4.14: Regional Reduced to Pole magnetic anomaly map and the 3D Euler inversion Pole.

4.2.2 Regional Cross Section

A regional profile (Figure 4.15) was selected in two segments, A – A`` and B – B`. The A – A" profile extends the GAIT 99 -21 Garzón thrust fault profile to the southeast. The profile was offset to the B – B` profile in order to cross the imbricate thrust zone mapped by Ingeominas geologists (Figures 4.10 and 4.11). The cross section contains Garzón Massif Complex units, fluvial/alluvial conglomerates of the Pepino Fm, and Orito Gp. sandstones. Rocks of the Pepino Formation and Orito Group are assumed to be late Eocene to early Oligocene in age (>25 Ma).

The steep gravity gradient on the NW flank of the Garzón Massif is interpreted as produced by dense granitic basement rocks thrust over low density sediments of the Upper Magdalena Valley on the Garzón thrust fault (Figure 4.15). The low relief anomalies to the SE are interpreted to reflect uniformly shallow basement rocks and thin crust. The observed gravity does not require crustal thickening under the Garzón Massif. In the magnetic model (Figure 4.15), the low magnetic anomalies over the SE flank of the Massif are produced by non-magnetic (low susceptibility) Precambrian sediments in a basement graben.

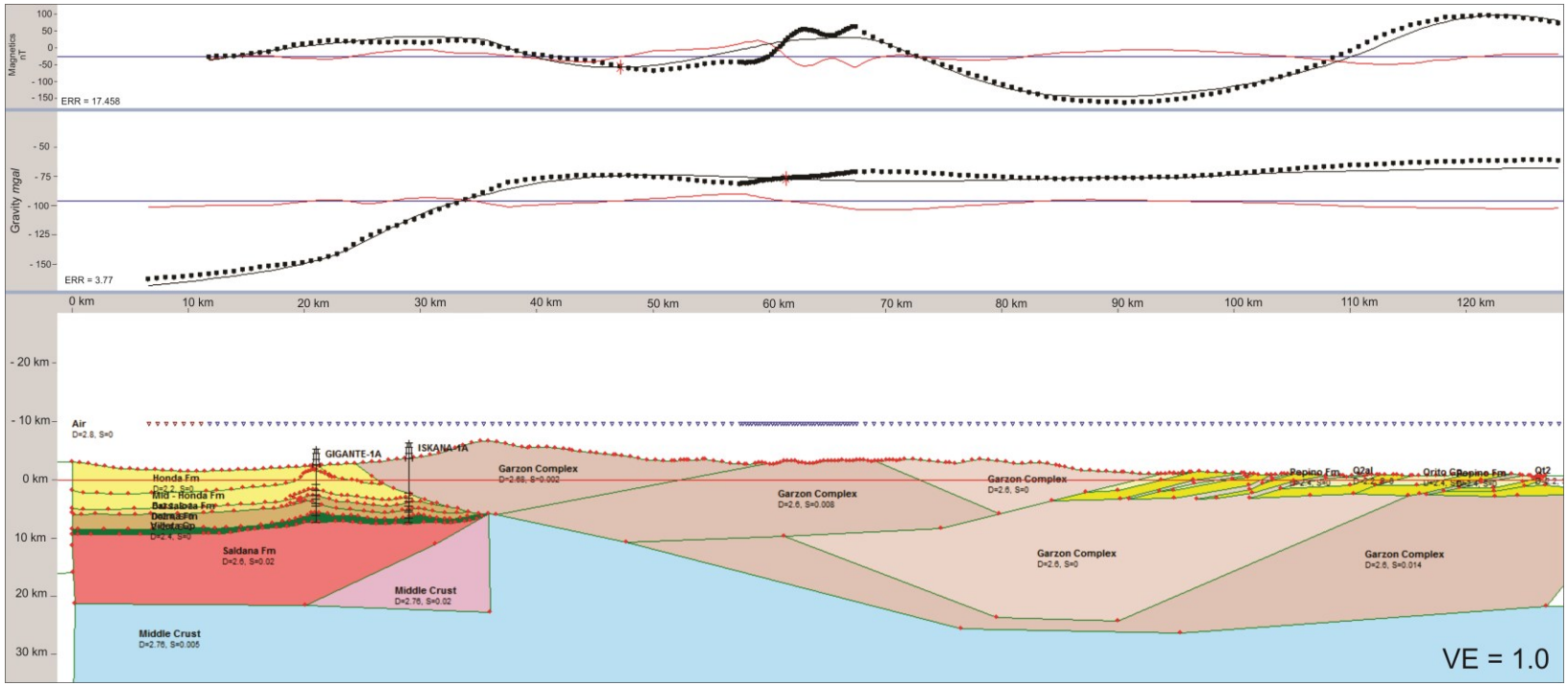

Figure 4.15: Density and magnetic model for regional profile. Calculated solid – black line, observed dotted – line, error red – line. See figures 4.10 and 4.11 for the location.

4.2.3 Tectonic Evolution of the Garzón Massif (25 Ma to Present)

To develop a model for the evolution of the Garzón Massif, a present-day structural interpretation was created and then retrodeformed. The GAIT 99-21 segment of the regional profile was interpreted based on seismic and well control (Figure 4.16). This structural interpretation was then extended to a schematic regional geologic model constrained by surface geology, gravity and magnetic data (Figures 4.15 and 4.17).

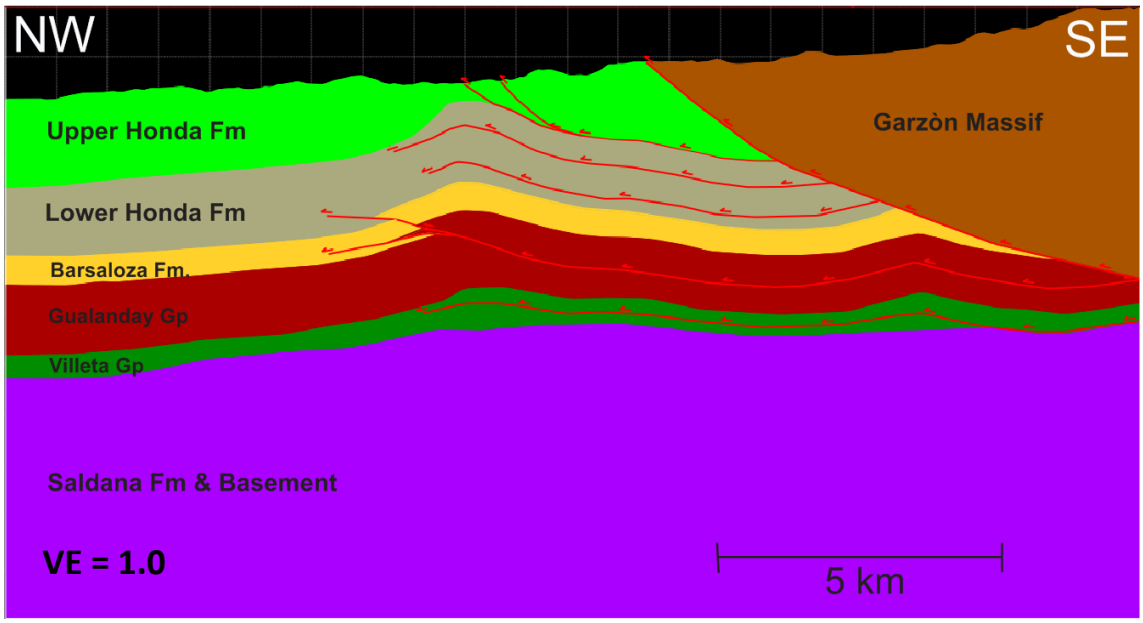

Figure 4.16: Structural model generated in Midland Valley Move software with the interpreted two dimensional GAIT – 99 – 21 seismic profile line and its formation tops.

To retrodeform the Garzón uplift, first, the minimum displacement was removed from the Garzón basement thrust and the basement thrust on the SE flank of the Massif assuming simple shear (Figure 4.18). Minimum slip on the Garzón thrust was 13 km. Vertical structural relief is at least 7 km. It is predicted to ramp up from a lower crustal detachment at a depth of about 20 km. Slip on the SE marginal basement thrust is

estimated at 9 km, but this is poorly constrained. The timing of the primary displacement on the Garzón thrust is fairly well constrained by sedimentary and radiometric data to be Andean, i.e., within the last 12 Ma (Van der Wiel, 1991). Timing of slip on the SE marginal basement thrust is also assumed to be within the last 12 Ma.

The sediments of the Pepino Formation and Orito Group, exposed in imbricate thrusts on the SE flank of the Massif are dated as >25 Ma, late Eocene to early Oligocene. Thus, the southeastward verging "thin-skinned" thrusting must have been post early Oligocene or < 25 Ma. Minimum shortening by thin-skinned thrusting is estimated at 43 km. A retrodeformed model prior to the thrusting at 25 Ma is shown in Figure 4.19. It should be noted that the thin-skinned shortening estimate is very approximate and sensitive to the dips on the imbricate ramps. It should therefore be tested by detailed mapping of the imbricate thrust zone. Timing of the thrusting is assumed to be 12 to 25 Ma.

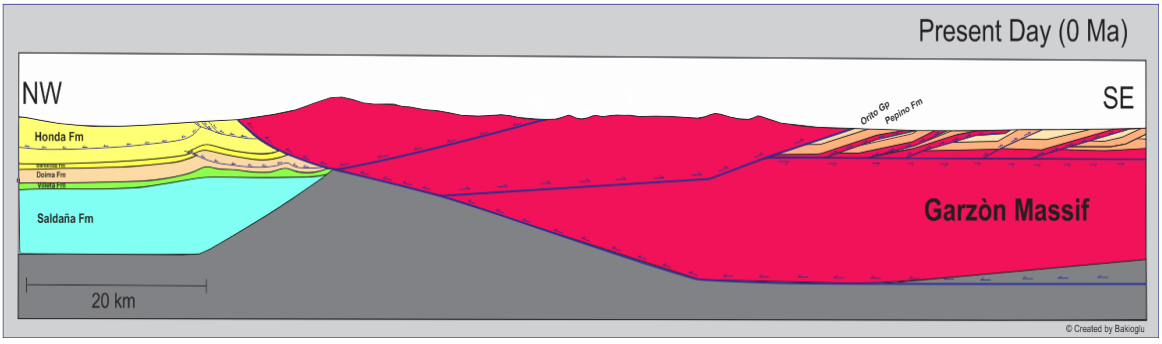

Figure 4.17: Present Day regional cross section of the Garzón Massif.

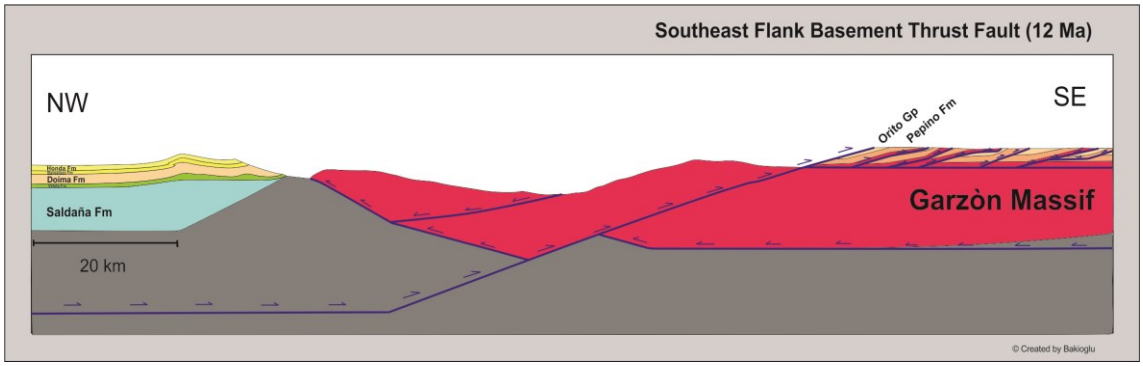

Figure 4.18: Retrodeformation at 12 Ma. Note symmetrical basement uplift on Garzón thrust and SE basement thrust faults. Total shortening = 22 km.

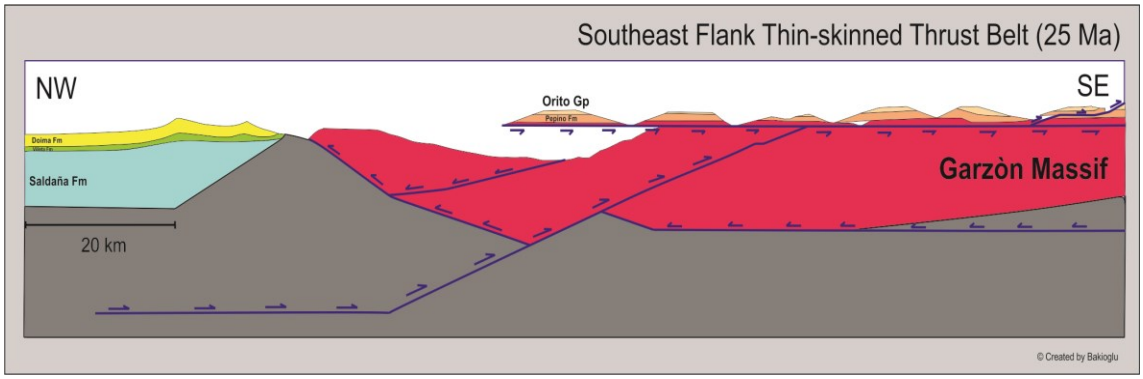

Figure 4.19: Retrodeformation at 25 Ma prior to southeastward thin – skinned thrusting. Total shortening = 43 km.

CHAPTER 5: CONCLUSIONS

The Garzón Massif, an active basement uplift with well, seismic, gravity, and magnetic data available, is an analog for Laramide style basement uplifts. Unlike many Laramide Rocky Mountain structures that were overprinted by extensional deformation, the Garzón fault is still an active thrust. In the past 12 Ma, PreCambrian age granitic rocks of the Garzón Massif have been uplifted and thrust over Cretaceous and Tertiary sediments of the Upper Magdalena Valley along the Garzón fault.

Gravity analysis indicates that the Garzón fault is a basement thrust fault dipping at a shallow angle under the Massif. Best-fit models show a true dip of 12 to 17 degrees to the southeast. This low angle thrust solution is supported by the measured 17 degree dip in the Iskana-1 well for the sediments under the Garzón fault. It is also in agreement with the most common dip angles found for 10 exploration wells that drilled through Precambrian overthrusts in the Laramide Rocky Mountains (Gries, 1983). The results support theoretical and experimental results that show that thrust dip angles can be explained by Anderson(1930)'s theory of Mohr-Coulomb failure for both crystalline and sedimentary rocks subjected to horizontal maximum compressive stress and vertical minimum stress.

The Garzón Massif is asymmetric with a deep sedimentary basin (Upper Magdalena Valley) on its NW flank.

Retrodeformed 2D regional models indicate at least 13 km of shortening and 7 km of uplift on the Garzón basement thrust and approximately 9 km of shortening on the SE marginal basement thrust fault in the last 12 Ma. This was preceded by approximately 43 km of shortening by thin-skinned imbricate thrusting to the southeast (12 - 25 Ma).

Euler deconvolution of the magnetic field shows pronounced NE-SW trending features under the Massif which are interpreted as faults bounding a possible pre-Cambrian sedimentary rift graben.

The observed gravity does not require crustal thickening under the Garzón Massif, and the Garzón thrust is predicted to ramp up from a lower crustal detachment at a depth of about 20 km. These predictions are compatible with seismic and gravity results for the Wind River thrust and recent passive source crustal imaging of the Bighorns Arch Seismic Experiment (BASE) that show no apparent crustal root or offset of the Moho under the uplifts (Yeck et al., 2013; Smithson et al., 1979). Detachments are also predicted in the lower crust (26 to 36 km) for the two Laramide uplifts.

REFERENCES

Agencia Nacional de Hidrocarburos. (2010). *Mapa de anomalias de bouguer total de la Republica de Colombia* [map]. Bogota, Colombia : Graterol, V.R.

Altenberger, U., Gunter, C., Meija Jimenez, D. M., Oberhansli, R., Scheffer, F., Sierra Rodriguez, G. I. (2012). The Garzón Massif, Colombia – a new ultrahigh – temperature metamorphic complex in the Early Neoproterozoic of Northern South America. *Mineralogy and Petrology, 106(3-4), 171 – 185.*

Berg, R. R. (1962). Mountain flank thrusting in Rock Mountain Foreland, Wyoming and Colorado. *Bulletin of the American Association of Petroleum Geologists*, 46 (11), 2019 – 2032.

Buitrago, J. (1994). The Petroleum system: From source to trap. In Chapter 30: Part V. *Petroleum Systems of the Neiva Area, Upper Magdalena Valley, Colombia. Case Studies--Western Hemisphere* (pp.483 – 497). Tulsa: Magoon & Dow.

Bustamante, C., Bayona G., Cardona, A., Gehrels, G., Mora, A., Valencia V. et al. (2010) U-Pb LA-ICP-MS Geochronology and Regional Correlation of Middle Jurassic Intrusive Rocks from the Garzón Massif, Upper Magdalena Valley and Central Cordillera, Colombia. *Boletin de Geologia, 32(2), 93 – 109.*

Butler, K. R. (1980). *Andean Type Foreland Deformation: Structural Development of Neiva Basin, Upper Magdalena Valley, Colombia.* Unpublished doctoral dissertation, University of South Carolina, Columbia.

Carson Services, Inc. (2000). *Airborne gravity and magnetic survey: Guadalupe – Acevedo – Matambo and Gaitanas blocks Colombia* (Technical Interpretation Report for Total Exploratie en Produktie Mij B.V Sucursal. Liberty Hill, TX, USA: Graterol, V.

Chorowicz, J., Chotin, P., Guillande, R. (1996*).* The Garzón fault: active southwestern boundary of the Caribbean Plate in Colombia. *Geologische Rundschau, 85(1), 172 – 179.*

Cordani, U.G., Cardona A., Jimenez D. M., Liu, D., Nutman, A.P. (2005). Geochronology of Proterozoic basement inliers in the Colombian Andes: Tectonic history of remnants of a fragmented Grenville belt. *Geological Society of London, Special Publication, 246, 329-346.*

Erslev, E.A. (2013). Formation and fracturing of Laramide basins. *Geological Society of America Abstracts with Programs, 45(7), 669.*

Foulger, G.R., Pierce, C. (n.d). Geophysical methods in geology. Retrieved March 15, 2014, from http://www.dur.ac.uk/g.r.foulger/Teaching/GG_HandoutsAll.pdf

Gries, R. (1983). Oil and gas prospecting beneath Precambrian of foreland thrust plates in Rocky Mountains. *The American Association of Petroleum Geologists Bulletin, 67(1), 1 – 28.*

Horton, B. K. , Mora, A., Nie, J., Parra, M., Reyes – Harker, A., Saylor, J.E et all. (2010). Linking sedimentation in the Northern Andes to basement configuration, Mesozoic extension, and Cenozoic shortening: Evidence from detrital zircon U – Pb Ages, Eastern Cordillera, Colombia. Retrieved November 15, 2012, from the website of Institute for Geophysics, University of Texas at Austin: http://www.ig.utexas.edu/people/staff/horton/publications/Horton_etal_GSAB_2010_.pdf

HOCOL S.A by Datalog Colombia LTDA. (2002). *End of Well, Report: ISKANA – 1A.* Bogota, Colombia: HOCOL S.A.

Howe, M. W. (1974). Nonmarine Neiva Formation (Pliocene?), Upper Magdalena Valley, Colombia. *Geological Society of America Bulletin, 85, 1031 – 1042.*

Hubbert, M. K. (1951). Mechanical basis for certain familiar geologic structures. *Bulletin of the Geological Society of America, 62, 355 – 372.*

Hurich, A. C., Smithson, S. B. (1982). Gravity interpretation of the southern Wind River Mountains, Wyoming. *Geophysics, 47(11), 1550 – 1561.*

Jaime, E., de Freitas, M. (2004). An Albian – Cenomanian unconformity in the Northern Andes: Evidence and tectonic significance. *Journal of South American Earth Sciences, 21(4), 466 -492.*

Jimenez-Meija, D.M., Cordani, U.G., Juliani, C. (2006). P-T-t conditions of high-grade metamorphic rocks of the Garzón massif, Andean basement, SE Colombia. *Journal of South American Earth Sciences, 21, 322–336.*

Labuz, J.F., Zang, A. (2012). ISRM Suggested Method, Mohr – Coulomb Failure Criterion. *Rock Mechanics and Rock Engineering, 45(6), 975 – 979.*

Mora, A., Blanco, M., Ferreira da Silva, S., Jaramillo, C., Parra, M., Strecker, M.R. The Eastern foothills of the Eastern Cordillera of Colombia: An example of multiple factors controlling structural styles and active tectonics. *GSA Bulletin, 122(11/12), 1846 – 1864.*

Nafe Drake Curve. (n.d). Retrieved on March 15, 2013 from http://gravity.wikia.com/wiki/Nafe-Drake_Curve

Narr, W. (1993). Deformation of Basement in Basement – Involved, Compressive Structures. *GSA Special Papers, 280,107 – 124.*

Narr, W., Suppe, J. (1994). Kinematic of Basement – Involved Compressive Structures. *American Journal of Science, 294, 802 – 860.*

Priem, H.N.A., Boelrijk, N.A.I.M., Hebeda, E.H., Kroonenberg, S.B. (1989). Rb-Sr and K-Ar evidence for the presence of a 1.6 Ga basement underlying the 1.2 Ga Garzón-Santa Marta granulite belt in the Colombian Andes. *Precambrian Research, 42(3–4), 315–324.*

Republica de Colombia Ministerio de Minas y Energia. [Tapias, J.G, Avella, M.L.T, Diederix, H., Guevera, G.N., Jimenez – Meija, D.M., Naranjo, J.A.O.]. (2007). Atlas Geologico de Colombia Plancha 5 – 14 [map]. 1:1.000.000

Restrepo - Pace, P.A., Colmenares, F., Higuera, C., Mayorga, M. (2004). A Fold – and – thrust belt along the western flank of the Eastern Cordillera of Colombia – Style, kinematics, and timing constraints derived from seismic data and detailed surface mapping (in Thrust tectonics and hydrocarbon systems, McClay). *AAPG Memoir, 82, 598 – 613.*

Restrepo – Pace, P.A., Cosca, M., Gehrels, G.E., Ruiz J. (1997). Geochronology and Nd isotopic data of Greenville – age rocks in Colombian Andes: New constraints for Late Proterozoic – Early Paleozoic paleocontinental reconstruction of the Americas. *Earth and Planetary Science Letters, 150 (3 – 4), 427 – 441.*

Roure, F., Colletta, B., Faure, J.L., Macellari, C., Osorio, M. (2005). Structural evolution and coupled kinematic-thermal modeling of the Upper Magdalena Basin in the vicinity of the Garzón Massif, Colombia. *Abstracts: Annual Meeting - American Association of Petroleum Geologists, 14*

Servicio Geologico Colombiano [Nuñez Tello, A., Carlos Julio, C.A., Francisco Alberto, V.A., Juan Carlos, C.A.]. (2001). Geología de la plancha 345 Campoalegre [map]. 1:100.000. Retrieved from http://aplicaciones1.ingeominas.gov.co/sicat/html/Metadato.aspx?CID=123120

Servicio Geologico Colombiano [Rodriguez, G.,Ferreira, P., Francisco Alberto, V.A., Nuñez Tello, A.]. (1998). Geología de la plancha 366 Garzón [map]. 1:100.000. Retrieved from http://aplicaciones1.ingeominas.gov.co/sicat/html/Metadato.aspx?CID=147942

Servicio Geologico Colombiano [Rodriguez, G.,Marta Edith, V.D., Zapata Garcia, G.].(2003). Geología de la Plancha 367 Gigante [map]. 1:100.000. Retrieved from http://aplicaciones1.ingeominas.gov.co/sicat/html/Metadato.aspx?CID=154114

Servicio Geologico Colombiano [Rodriguez, G.,Marta Edith, V.D., Zapata Garcia, G.].(2003). Geología de la Plancha 368 San Vicente del Caguán [map]. 1:100.000. Retrieved from http://aplicaciones1.ingeominas.gov.co/sicat/html/Metadato.aspx?CID=154115

Servicio Geologico Colombiano [Rodriguez, G.,Marta Edith, V.D., Zapata Garcia, G.]. (2003). Geología de la Plancha 389 Timaná [map]. 1:100.000. Retrieved from http://aplicaciones1.ingeominas.gov.co/sicat/html/Metadato.aspx?CID=154116

Servicio Geologico Colombiano [Rodriguez, G.,Marta Edith, V.D., Zapata Garcia, G.]. (2003). Geología de la Plancha 389 Timaná [map]. 1:100.000. Retrieved from http://aplicaciones1.ingeominas.gov.co/sicat/html/Metadato.aspx?CID=154116

Servicio Geologico Colombiano [Rodriguez, G.,Marta Edith, V.D., Zapata Garcia, G.]. (2003). Geología de la Plancha 390 Puerto Rico [map]. 1:100.000. Retrieved from http://aplicaciones1.ingeominas.gov.co/sicat/html/Metadato.aspx?CID=154117

Servicio Geologico Colombiano [Rodriguez, G.,Marta Edith, V.D., Zapata Garcia, G.]. (2003). Geología de la Plancha 391 Lusitania [map]. 1:100.000. Retrieved from http://aplicaciones1.ingeominas.gov.co/sicat/html/Metadato.aspx?CID=154118

Skeen, R. C., Ray, R.R. (1983). Seismic Models and Interpretation of the Casper Arch Thrust: Application to Rocky Mountain Foreland Structure. *In Rocky Mountain Foreland Basins and Uplifts. Association of Geologists (pp. 99 – 124). from J.D Lowell*

Smithson, S. B., Brewer, J., Hurich, C., Kaufman, S., Oliver, J. (1987). Nature of the Wind River thrust, Wyoming, from COCORP deep – reflection data and from gravity data. *Geology, 6, 648 – 652.*

Telford, W. M., Geldart, L.P, Sheriff, R.E. (1990). *Applied Geophysics* (2nd ed.). New York: Cambridge University Press.

Van Der Wiel, A. M. (1991). *Uplift and Volcanism of the SE Colombian Andes in Relation to Neogene Sedimentation of the Upper Magdalena Valley.* Unpublished doctoral dissertation, University of Utrecth, Utrecht.

Van Der Wiel, A.M., Vam Der Bergh, G.D. (1992). Uplift, subsidence and volcanism in the southern Neiva Basin, Colombia, Part 1: Influence on fluvial deposition in the Miocene Honda Formation. *Journal of South American Earth Sciences, 5, 157 – 173.*

Van Der Wiel, A. M., Van Den Bergh, G. D. (1992). Uplift, subsidence and volcanism in the southern Neiva Basin, Colombia, Part 2: Influence on fluvial deposition in the Miocene Gigante Formation. *Journal of South American Earth Sciences, 5, 175-196.*

Van Der Wiel, A.M. (1990). Uplift age of the Garzón Massif (Eastern Cordillera, S. Colombia) in relation to the infill of the adjacent S. Neiva basin. *Colloques Et Seminaires - Institut De Recherche Scientifique Pour Le Developpement En Cooperation,* 217-218.

Worthington, L.L, Erslev, E.A., Miller, K.C, Sheenan, A.F., Yeck, W.L. (2012). [Crustal thickness and velocity structure across the Bighorn Mountains, Northern Wyoming: Insights into Laramide – style orogenesis from the Bighorn Arch Seismic Experiment (BASE), *2012 IRIS Workshop*]. Retrieved May 15, 2014, from http://www.iris.edu/hq/iris_workshop2012/scihi/WebPages/0032.html

Yeck, W.L., Anderson, M., Ball, J., Erslev, E.A., Miller, K., Siddoway, C. S. et al. (2013). Basin and crustal structure of the Bighorn Mountain Region from teleseismic receiver function and surface wave analysis: Implications for the kinematics of Laramide shortening. *Geological Society of America Abstracts with Programs, 45(7), 669.*

Zawislak, L. R., Smithson, S. B. (1981). Problems of interpretation of COCORP deep seismic reflection data, Wind River range, Wyoming. *Geophysics, 46(12), 1684 – 1701.*

APPENDIX A: MODEL COMPARISONS TO FIND OUT THE BEST FITTED ON GARZÓN FAULT

Since the best fit model for the Garzón fault dip also varies with the density input for the Garzón Massif polygon, the misfit errors were calculated for 11 densities from 2.60 to 2.70 gr/cm^3 and for 8 apparent fault dip angles from horizontal to 35 degrees (Table A.1 and Chart A.1). For increasing density values for the Garzón polygon, the best-fit fault dip angle declined. For example, for a Garzón density of 2.61 gr/cm^3, the best-fit fault dip angle is 35 degrees (1.11 error). For a density of 2.69 gr/cm^3, the best-fit fault dip angle is 0 degrees or horizontal (1.06 error). The errors for the best-fit densities for each dip angle tested are highlighted in red (Table A.1).

Table A.1: Misfit errors for Garzón thrust for 8 dip angles and 11 densities. Errors for best – fit density for each dip angle shown in red. Solutions for density of 2.64 g/cm^3 highlighted yellow.

Density (g/cm3)	0 Degree	5 Degree	10 Degree	15 Degree	20 Degree	25 Degree	30 Degree	35 Degree
2.60	3.41	2.68	2.11	1.75	1.60	1.41	1.33	1.28
2.61	3.08	2.33	1.76	1.42	1.30	1.17	1.13	1.11
2.62	2.76	1.99	1.45	1.18	1.11	1.08	1.10	1.12
2.63	2.44	1.68	1.20	1.07	1.09	1.19	1.26	1.32
2.64	**2.13**	**1.40**	**1.07**	**1.14**	**1.24**	**1.44**	**1.55**	**1.64**
2.65	1.84	1.18	1.09	1.34	1.52	1.78	1.91	2.01
2.66	1.57	1.06	1.26	1.65	1.86	2.16	2.32	2.42
2.67	1.33	1.07	1.52	2.00	2.24	2.57	2.74	2.85
2.68	1.15	1.21	1.85	2.39	2.64	3.00	3.18	3.30
2.69	1.06	1.45	2.20	2.79	3.06	3.43	3.62	3.74
2.70	1.07	1.73	2.57	3.20	3.48	3.87	4.07	4.20

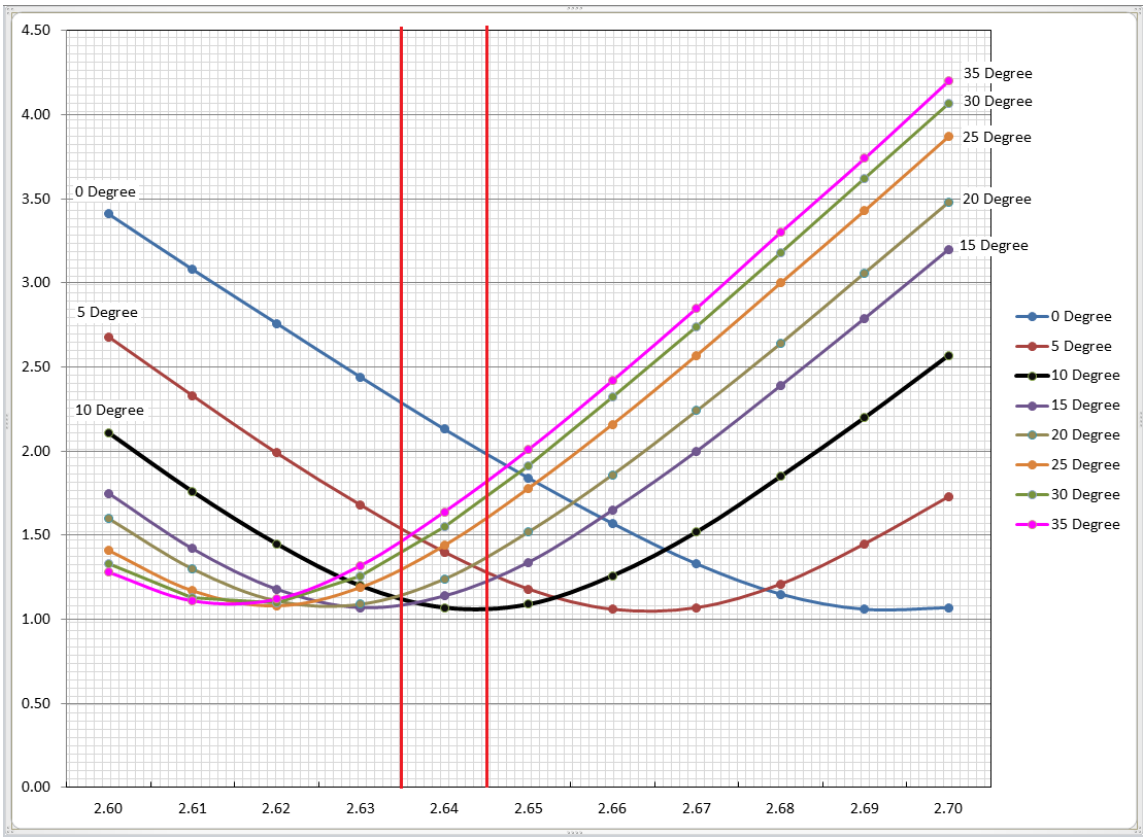

Chart A.1: Misfit errors for Garzón thrust models for 8 dip angles and 11 densities. Errors for 10 dip angle and2.64g/cm^{3}density are highlighted.